

Contributions to 2nd TeV Particle Astrophysics Conference (TeV PA II)

Madison Wisconsin - 28-31 August 2006

IceCube Collaboration

A. Achterberg³¹, M. Ackermann³³, J. Adams¹¹, J. Ahrens²¹, K. Andeen²⁰, D. W. Atlee²⁹,
 J. N. Bahcall²⁵(deceased), X. Bai²³, B. Baret⁹, S. W. Barwick¹⁶, R. Bay⁵, K. Beattie⁷,
 T. Becka²¹, J. K. Becker¹³, K.-H. Becker³², P. Berghaus⁸, D. Berley¹², E. Bernardini^{33*},
 D. Bertrand⁸, D. Z. Besson¹⁷, E. Blaufuss¹², D. J. Boersma²⁰, C. Bohm²⁷, J. Bolmont³³,
 S. Böser³³, O. Botner³⁰, A. Bouchta³⁰, J. Braun²⁰, C. Burgess²⁷, T. Burgess²⁷,
 T. Castermans²², D. Chirkin⁷, B. Christy¹², J. Clem²³, D. F. Cowen^{29,28}, M. V. D'Agostino⁵,
 A. Davour³⁰, C. T. Day⁷, C. De Clercq⁹, L. Demirörs²³, F. Descamps¹⁴, P. Desiati²⁰,
 T. DeYoung²⁹, J. C. Diaz-Velez²⁰, J. Dreyer¹³, J. P. Dumm²⁰, M. R. Duvoort³¹,
 W. R. Edwards⁷, R. Ehrlich¹², J. Eisch²⁶, R. W. Ellsworth¹², P. A. Evenson²³, O. Fadiran³,
 A. R. Fazely⁴, T. Feser²¹, K. Filimonov⁵, B. D. Fox²⁹, T. K. Gaisser²³, J. Gallagher¹⁹,
 R. Ganugapati²⁰, H. Geenen³², L. Gerhardt¹⁶, A. Goldschmidt⁷, J. A. Goodman¹²,
 R. Gozzini²¹, S. Grullon²⁰, A. Groß¹⁵, R. M. Gunasingha⁴, M. Gurtner³², A. Hallgren³⁰,
 F. Halzen²⁰, K. Han¹¹, K. Hanson²⁰, D. Hardtke⁵, R. Hardtke²⁶, T. Harenberg³², J. E. Hart²⁹,
 T. Hauschildt²³, D. Hays⁷, J. Heise³¹, K. Helbing³², M. Hellwig²¹, P. Herquet²², G. C. Hill²⁰,
 J. Hedges²⁰, K. D. Hoffman¹², B. Hommez¹⁴, K. Hoshina²⁰, D. Hubert⁹, B. Hughey²⁰,
 P. O. Hulth²⁷, K. Hultqvist²⁷, S. Hundertmark²⁷, J.-P. Hülß³², A. Ishihara²⁰, J. Jacobsen⁷,
 G. S. Japaridze³, H. Johansson²⁷, A. Jones⁷, J. M. Joseph⁷, K.-H. Kampert³², A. Karle²⁰,
 H. Kawai¹⁰, J. L. Kelley²⁰, M. Kestel²⁹, N. Kitamura²⁰, S. R. Klein⁷, S. Klepser³³,
 G. Kohnen²², H. Kolanoski⁶, L. Köpke²¹, M. Krasberg²⁰, K. Kuehn¹⁶, H. Landsman²⁰,
 H. Leich³³, D. Leier¹³, M. Leuthold¹, I. Liubarsky¹⁸, J. Lundberg³⁰, J. Lünemann¹³,
 J. Madsen²⁶, K. Mase¹⁰, H. S. Matis⁷, T. McCauley⁷, C. P. McParland⁷, A. Meli¹³,
 T. Messarius¹³, P. Mészáros^{29,28}, H. Miyamoto¹⁰, A. Mokhtarani⁷, T. Montaruli^{20,34},
 A. Morey⁵, R. Morse²⁰, S. M. Movit²⁸, K. Münich¹³, R. Nahnauer³³, J. W. Nam¹⁶,
 P. Nießen²³, D. R. Nygren⁷, H. Ögelman²⁰, A. Olivas¹², S. Patton⁷, C. Peña-Garay²⁵,
 C. Pérez de los Heros³⁰, A. Piegsa²¹, D. Pieloth³³, A. C. Pohl³⁰, R. Porrata⁵, J. Pretz¹²,
 P. B. Price⁵, G. T. Przybylski⁷, K. Rawlins², S. Razzaque^{29,28}, E. Resconi¹⁵, W. Rhode¹³,
 M. Ribordy²², A. Rizzo⁹, S. Robbins³², P. Roth¹², C. Rott²⁹, D. Rutledge²⁹, D. Ryckbosch¹⁴,
 H.-G. Sander²¹, S. Sarkar²⁴, S. Schlenstedt³³, T. Schmidt¹², D. Schneider²⁰, D. Seckel²³,
 S. H. Seo²⁹, S. Seunarine¹¹, A. Silvestri¹⁶, A. J. Smith¹², M. Solarz⁵, C. Song²⁰, J. E. Sopher⁷,
 G. M. Spiczak²⁶, C. Spiering³³, M. Stamatikos²⁰, T. Stanev²³, P. Steffen³³, T. Stezelberger⁷,
 R. G. Stokstad⁷, M. C. Stoufer⁷, S. Stoyanov²³, E. A. Strahler²⁰, T. Straszheim¹²,
 K.-H. Sulanke³³, G. W. Sullivan¹², T. J. Sumner¹⁸, I. Taboada⁵, O. Tarasova³³, A. Tepe³²,
 L. Thollander²⁷, S. Tilav²³, M. Tluczykont³³, P. A. Toale²⁹, D. Turčan¹², N. van Eijndhoven³¹,
 J. Vandebroucke⁵, A. Van Overloop¹⁴, B. Voigt³³, W. Wagner²⁹, C. Walck²⁷, H. Waldmann³³,
 M. Walter³³, Y.-R. Wang²⁰, C. Wendt²⁰, C. H. Wiebusch¹, G. Wikström²⁷, D. R. Williams²⁹,
 R. Wischnewski³³, H. Wissing¹, K. Woschnagg⁵, X. W. Xu⁴, G. Yodh¹⁶, S. Yoshida¹⁰,
 J. D. Zornoza²⁰

¹III Physikalisches Institut, RWTH Aachen University, D-52056, Aachen, Germany

²Dept. of Physics and Astronomy, University of Alaska Anchorage, 3211 Providence Dr., Anchorage, AK

99508, USA

³CTSPS, Clark-Atlanta University, Atlanta, GA 30314, USA

⁴Dept. of Physics, Southern University, Baton Rouge, LA 70813, USA

⁵Dept. of Physics, University of California, Berkeley, CA 94720, USA

⁶Institut für Physik, Humboldt Universität zu Berlin, D-12489 Berlin, Germany

⁷Lawrence Berkeley National Laboratory, Berkeley, CA 94720, USA

⁸Université Libre de Bruxelles, Science Faculty CP230, B-1050 Brussels, Belgium

⁹Vrije Universiteit Brussel, Dienst ELEM, B-1050 Brussels, Belgium

¹⁰Dept. of Physics, Chiba University, Chiba 263-8522 Japan

¹¹Dept. of Physics and Astronomy, University of Canterbury, Private Bag 4800, Christchurch, New Zealand

¹²Dept. of Physics, University of Maryland, College Park, MD 20742, USA

¹³Dept. of Physics, Universität Dortmund, D-44221 Dortmund, Germany

¹⁴Dept. of Subatomic and Radiation Physics, University of Gent, B-9000 Gent, Belgium

¹⁵Max-Planck-Institut für Kernphysik, D-69177 Heidelberg, Germany

¹⁶Dept. of Physics and Astronomy, University of California, Irvine, CA 92697, USA

¹⁷Dept. of Physics and Astronomy, University of Kansas, Lawrence, KS 66045, USA

¹⁸Blackett Laboratory, Imperial College, London SW7 2BW, UK

¹⁹Dept. of Astronomy, University of Wisconsin, Madison, WI 53706, USA

²⁰Dept. of Physics, University of Wisconsin, Madison, WI 53706, USA

²¹Institute of Physics, University of Mainz, Staudinger Weg 7, D-55099 Mainz, Germany

²²University of Mons-Hainaut, 7000 Mons, Belgium

²³Bartol Research Institute, University of Delaware, Newark, DE 19716, USA

²⁴Dept. of Physics, University of Oxford, 1 Keble Road, Oxford OX1 3NP, UK

²⁵Institute for Advanced Study, Princeton, NJ 08540, USA

²⁶Dept. of Physics, University of Wisconsin, River Falls, WI 54022, USA

²⁷Dept. of Physics, Stockholm University, SE-10691 Stockholm, Sweden

²⁸Dept. of Astronomy and Astrophysics, Pennsylvania State University, University Park, PA 16802, USA

²⁹Dept. of Physics, Pennsylvania State University, University Park, PA 16802, USA

³⁰Division of High Energy Physics, Uppsala University, S-75121 Uppsala, Sweden

³¹Dept. of Physics and Astronomy, Utrecht University/SRON, NL-3584 CC Utrecht, The Netherlands

³²Dept. of Physics, University of Wuppertal, D-42119 Wuppertal, Germany

³³DESY, D-15735 Zeuthen, Germany

³⁴on leave of absence University of Bari, 70126, Italy

Table of Contents

- (i) Kael Hanson for the IceCube collaboration, Construction Status and Future of the IceCube Neutrino Observatory
- (ii) Julia K. Becker for the IceCube collaboration, Implications of AMANDA Neutrino Flux Limits
- (iii) D.F. Cowen for the IceCube collaboration, Tau Neutrinos in IceCube
- (iv) Elisa Resconi for the IceCube collaboration, IceCube: Multiwavelength Search for Neutrinos from Transient Point Sources
- (v) Xinhua Bai and Thomas K. Gaisser for the IceCube collaboration, Air Showers in a Three-Dimensional Array: Recent Data from IceCube/IceTop
- (vi) Juan de Dios Zornoza for the IceCube collaboration, High-Energy Gammas from the Giant Flare of SGR 1806-20 of December 2004 in AMANDA
- (vii) Jon Dumm and Hagar Landsman for the IceCube collaboration, IceCube – First Results
- (viii) Jessica Hodges for the IceCube collaboration, Multi-Year Search for a Diffuse Flux of Muon Neutrinos with AMANDA-II
- (ix) Brennan Hughey for the IceCube collaboration, Searches for Neutrinos from Gamma-Ray Bursts with AMANDA-II and IceCube

Construction Status and Future of the IceCube Neutrino Observatory

Kael D. Hanson¹ for the IceCube Collaboration

¹ A3RI, University of Wisconsin - Madison, 222 W. Washington Ave, Madison, WI 53703

Abstract. The IceCube neutrino telescope nears the end of its second running season having collected a sample of over 2×10^9 triggered events. While the majority of these events are cosmic ray muons, the detector is already sufficiently well understood to allow identification of neutrino-induced muon candidate events from the CR background. The production of optical module instrumentation is now well-established, the modules themselves are functioning properly with low failure rate, and it has been proven that the hot water drill can deliver the holes needed for deployment of these instruments. The project plans to deploy 12-14 strings each year during the next several austral summers to bring the detector volume to 1 km^3 .

1. Introduction

High-energy neutrino astrophysics is entering the era of kilometer-scale observatories. The IceCube neutrino telescope will be the first detector with an integrated exposure volume to reach $1 \text{ km}^3 \cdot \text{yr}$. The detector includes a deep array of digital optical sensors deployed at depths between 1500 m and 2450 m in holes drilled in the glacial ice sheet at the geographic South Pole. These deep sensor modules detect the Cherenkov light radiated by passing charged relativistic particles in transit through the ice medium. The optical properties of this medium have been measured with *in situ* light sources [1] deployed with the predecessor detector array, AMANDA [2, 3]: below 1500 m the ice becomes bubble free where long absorption and scattering lengths are found ($\ell_{\text{abs}} \sim 100 \text{ m}$, $\ell_{\text{scatt}} \sim 25 \text{ m}$).

The IceCube deep array is optimized for the detection of muons produced by high energy ($E \gg 1 \text{ TeV}$) neutrinos from astrophysical point source emitters such as active galactic nuclei or transient sources such as gamma ray bursts [4]. The muon is produced via charged-current interactions of the neutrino with ice nuclei ($\nu_\mu + N \rightarrow \mu + X$), typically exterior to the detector volume due to the long range of muons with energies in excess of 1 TeV. Ice is also an ideal calorimetric medium due to the long optical absorption lengths and so the visible energy of contained neutrino events can be reconstructed with $\pm 20\%$ resolution in the exponent. In addition to these high-energy phenomena of cosmic origin, IceCube may observe signals from dark matter annihilations and will collect a high statistics sample ($O(10^6)$) of atmospheric neutrinos relevant to particle physics topics such as Lorenz invariance tests in regions unreachable by other techniques. At the low energy end, IceCube presents an effective volume of approximately 2.0×10^6 tons to MeV neutrinos from supernovae.

An array of the same sensors deployed in the ice holes are frozen into tanks at the top of each hole, providing an airshower detector component for IceCube. Called IceTop, this instrumentation may be used as a trigger veto to assist in rejection of cosmic ray event backgrounds in the deep detector. Furthermore, combining its data with data from the deep-ice array provides a unique opportunity to study cosmic ray composition in the region of the “knee,” extending earlier measurements performed using the combination of the SPASE and AMANDA detectors [5, 6].

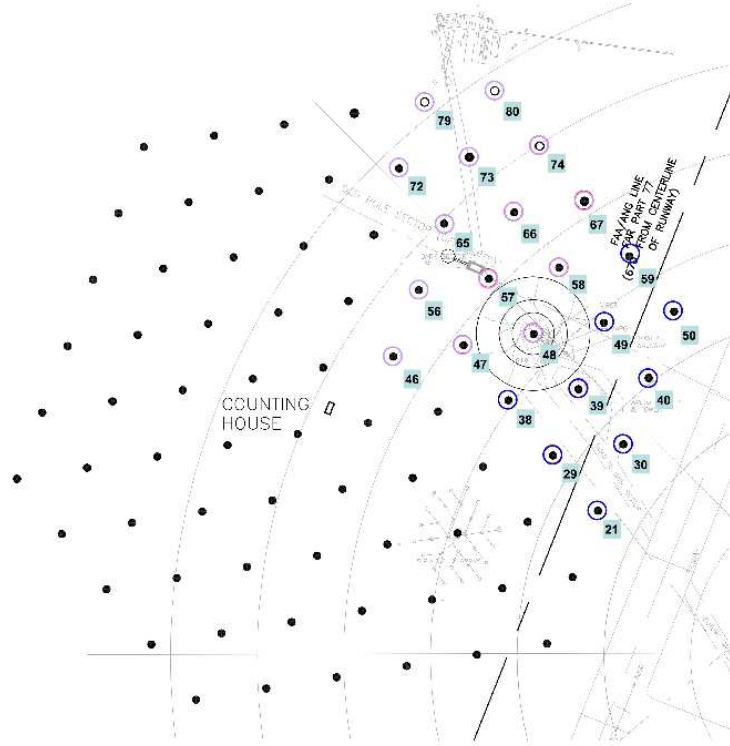


Figure 1. Surface view showing an overlay of the IceCube detector on the South Pole station map. The Amundsen-Scott station is slightly off the lower righthand corner of this illustration. The existing AMANDA detector is represented by the concentric circles centered approximately on hole #48. Thick dots represent planned hole locations, those circled are either existing or planned in the 2006-2007 deployment season.

2. Status of IceCube instrument deployment

The first IceCube string (#21) and the first four IceTop stations (#21, #29, #30, and #39) were deployed in January 2005 at the end of the deployment season and were operated during the austral winter of that year. The survivability of the digital optical modules during deployment and subsequent refreeze of the drill hole was established (all DOMs deployed during this season continue to function properly), useful performance data were gathered throughout the year of operation of the string [7, 8], and neutrino candidate events were selected from this data run.

During the following austral summer season, from December 2005 to January 2006, eight more strings (#29, #30, #38, #39, #40, #49, #50, and #59) and twelve more IceTop stations (#38, #40, #47, #48, #49, #50, #57, #58, #59, #66, #67, and #74) were deployed bringing the count to 9 strings and 16 surface stations and a total enclosed ice volume of 0.1 km^3 . Of the 604 sensors deployed to date, 597 of them communicate and 592 are producing high quality data. A current view of the IceCube detector installation is shown in Figure 1. The deployment plan calls for 12-14 strings and 10 surface stations to be deployed this year (2006-2007) to be followed by an average of 14 strings and IceTop stations in the following years until 2011 when the full complement of instrumentation will have been deployed, approximately 70-75 strings (60 DOMs per string) and 80 surface stations (4 DOMs per station). IceCube will be operated throughout the construction, achieving an integrated exposure of $1 \text{ km}^3 \cdot \text{yr}$ by 2009 and $4 \text{ km}^3 \cdot \text{yr}$ by the second year of operation with the completed detector. We anticipate that the total operating lifetime of the experiment will be 20 years.

3. Drilling and deployment

The Enhanced Hot Water Drill (EHWD) system delivers $2.5\text{ km} \times 60\text{ cm}$ holes to the deployment team for insertion of the optical sensor hardware. The system includes self-contained heating and electrical powerplants with a combined power of approximately 5 MW, pumping systems, a control facility, and drilling towers. Each year the drill camp is moved into place near the target holes. The towers then operate as mobile field facilities served by the central drill camp and towed into position atop each drill hole (Figure 2). During operation, the drill supplies 200 gallons per minute of $190\text{ }^{\circ}\text{C}$ water at 1000 psi. The average fuel consumed per hole is 7200 gallons. The entire operation of drilling a hole and deploying the optical module instrumentation takes approximately 50 hours.



Figure 2. IceCube drill camp with drill tower image inset in lower left corner. The tower sits atop a drill hole. Two icetop tanks forming a station are visible in trench to the right of the drill tower.

4. The IceCube digital optical module

The IceCube digital optical module (DOM) (Figure 3) is the central detector element used throughout the array, both in the deep ice and at the surface. It is a self-contained optical detector and data acquisition device. The analog optical device is a 10" photomultiplier tube running at 1.0×10^7 gain into a $\sim 50\text{ }\Omega$ front-end load impedance. PMT high voltage bias is supplied internally by a DC-DC converter module that is powered from the +5 V line on the DOM mainboard and can produce a programmable HV from 0 to +2048 V. A classical resistive divider bleeder distributes voltages to the PMT dynodes. The DOM also contains a PCB containing 12 405 nm LEDs which may be flashed in the ice to provide a known optical source for studying ice properties or performing geometrical calibrations of the sensor array. All components are housed inside a 0.5" thick glass pressure sphere rated to 10000 psi external pressure. The power and digital communication lines exit the DOM via the penetrator cable which attaches to the main communication cable bundles. DOM digital communication signals travel to the surface over copper quads contained within the 45 mm cable bundles.

DOMs are assembled at three production and test facilities worldwide within the IceCube collaboration: University of Wisconsin, Stockholm University / Uppsala University, and DESY Zeuthen. Following assembly each DOM undergoes a 2-3 week test at various temperatures from $+25\text{ }^{\circ}\text{C}$ to $-55\text{ }^{\circ}\text{C}$ in order to evaluate its performance at low temperature and to characterize various optical and electronic operational parameters [9]. All data thus far obtained with DOMs manufactured at all sites supports the claim that all sites are producing equivalent sensor hardware. To date 2000 of a total 5000 DOMs have been built. First pass yields are nearing 90% and the shipping yields are in excess of 95%.



Figure 3. IceCube digital optical module, shown here without mounting harness for clarity. The PCB stack is visible with the flasher board module obscuring most of the DOM mainboard. The HV generator module is mounted on the flasher board (partially blocked in this figure by the penetrator assembly). The photomultiplier tube faces downward and here is almost completely hidden under the PCBs.

5. Data acquisition

The PMT pulses are converted into digital waveforms by one or more digitizer chips at speeds up to 3×10^8 samples/s. Each DOM runs in self-triggered mode with the option to monitor digital trigger lines connected to its neighbor DOMs which it may use to influence the trigger decision. DOM-level triggers force a digitization and readout of the digitizers into local memory on the DOM (the DOM has a capacity of 16 MB) and each readout is time stamped with a counter value derived from the 40 MHz local DOM oscillator. Upon command from a surface controller, the DOM will transfer the contents of its memory buffers to the surface at a bit rate of 1 Mbit/s per copper pair.

At the surface, DOMs are readout by specialized PCI cards plugged into industrial PCs running Linux. Software running inside these computers must translate the DOM timestamp to a global quantity since each DOM oscillator is free running. Therefore the time stamp generated in the DOM is only locally relevant. The time transformation is achieved by a process called RAPCal wherein the DOM and the surface digital communication hardware periodically (approximately once per second) exchange analog pulses and stamp the arrival and departure times. This information is used to establish the DOM clock to surface clock mapping. The clocks at the surface are driven from a single 10 MHz master clock signal synchronized to GPS. Measurements in the laboratory and *in situ* at South Pole demonstrate that DOM-to-DOM time jitter is $O(3$ ns) less than the design specification of 5 ns.

Once the digitized PMT pulses have been stamped with a global time, they are merged and sorted into a stream which is sent over ethernet to a cluster of trigger and event processor computers. The triggering and event packaging is accomplished entirely in application software. During the 2006 run, two triggers were implemented: a minimum bias trigger (MBT) generating an event trigger every n -th hit for system debugging and the main trigger for physics analysis, the simple majority trigger (SMT), requiring coincidence of 8 or more DOMs hit in the deep-ice array or 6 or more hits in the IceTop array within a time window of 5 μ s. The triggers were formed in separate trigger processors for the in-ice and IceTop arrays; coincident triggers were then handled by a global trigger unit. Typical trigger rates from a run in mid-winter operation are listed in Table 1.

	MBT	SMT
In-Ice	5.28 Hz	139 Hz
IceTop	0.875 Hz	6.43 Hz
IceTop - In-Ice Coincident	0.25 Hz	

Table 1. Trigger rates from a June 23, 2006 data run.

6. Summary

IceCube is soon to begin its 3rd deployment season after concluding a successful deployment and running season. All indications from data quality verification studies point to the hardware functioning at or above its design specification. The detector will reach an integrated exposure volume of $1 \text{ km}^3 \cdot \text{yr}$ in as little as two years' time. Future detectors involving acoustic and radio detection techniques are being investigated as potential additions to the IceCube observatory to substantially extend the detector volume, particularly at higher energies.

References

- [1] Ackermann M et. al. Optical properties of deep glacial ice at the South Pole 2006 *J. Geophys. Res.* **111** D13203
- [2] Andres E et. al. Observation of high-energy neutrinos using Cherenkov detectors embedded deep in Antarctic ice 2001 *Nature* **410** 441–3
- [3] Ahrens J et. al. Observation of high energy atmospheric neutrinos with the Antarctic muon and neutrino detector array 2002 *Phys. Rev. D* **66** 012005
- [4] Ahrens J et. al. Sensitivity of the IceCube detector to astrophysical sources of high energy muon neutrinos. 2004 *Astropart. Phys.* **20** 507–32
- [5] Ahrens J et. al. Calibration and survey of AMANDA with the SPASE detectors 2004 *Nucl. Instr. Meth.* **A522** 347–59
- [6] Bai X and Gaisser T Air showers in a three dimensional array: recent data from IceCube/IceTop 2006 *this proceedings*
- [7] Achterberg A et. al. First year performance of the IceCube neutrino telescope 2006 *Astropart. Phys.* **26** 155–73
- [8] Dumm J and Landsman H IceCube - first results 2006 *this proceedings*
- [9] Hanson K and Tarasova O Design and production of the IceCube digital optical module 2006 *Proceedings of the 4th International Conference on New Developments in Photodetection* published in *Nucl. Instr. Meth.* **A567** 214–7

Implications of AMANDA neutrino flux limits

Julia Becker for the IceCube Collaboration¹

Universität Dortmund, Institut für Physik, 44221 Dortmund, Germany

E-mail: julia.becker@udo.edu

Abstract. The Antarctic Muon And Neutrino Detector Array (AMANDA) is currently the most sensitive neutrino telescope at high energies. Data have been collected in a period of eight years and analyzed with different analysis strategies. Limits to the neutrino flux from point sources, transient emissions, source catalogs and limits to different diffuse flux models have been obtained implying in some cases strong constraints to hadronic interaction models of such sources. In this contribution, implications of the diffuse neutrino limit will be discussed with respect to neutrino production mechanisms in astrophysical sources.

1. Neutrino flux predictions

The existence of Ultra High Energy Cosmic Rays (UHECRs) as well as the detection of TeV photon emissions from galactic and extragalactic sources are a strong indication for neutrino (ν) emission from the same sources. Pions and kaons are believed to take a fraction of the proton energy producing TeV photons in coincidence with high energy neutrinos. Although the atmospheric background of neutrinos is quite high, it decreases rapidly with energy ($\sim E^{-3.7}$) while the extraterrestrial spectra of galactic and extra-galactic sources are typically flatter (typically $\sim E^{-2}$ if shock acceleration is the main mechanism producing high energetic protons at the source). The latter should therefore become the dominant component of the total diffuse spectrum at a certain energy, which depends on the normalization of the neutrino flux. Different predictions are shown in Fig. 4. The left panel shows various calculations which use the diffuse X-ray background as measured by ROSAT to normalize the neutrino spectrum, see [1, 2]. This is justified when assuming the production of neutrinos along with X-rays at the foot of jets of Active Galactic Nuclei (AGN) where protons are accelerated into the photon target of the disk. The right panel shows models based on the correlation between UHECRs, TeV photons and neutrinos, see [7, 4]. Such sources are optically thin to both TeV photons and protons.

2. Detection techniques of AMANDA

AMANDA detects muon-neutrinos (ν_μ s) by observing secondary muons from charged current interactions of the neutrinos with the nucleons of the ice. The muons are traveling faster than light in ice and emit Cherenkov radiation which is detected by the photomultiplier tubes. Between the years 2000 and 2004 data from effectively 1001 days have been taken and a ν_μ sample of 4282 events from the Northern hemisphere has been collected². In order to keep the analysis blinded to avoid experimenter's bias, analyses cuts are optimized using off-source samples created by scrambling the right ascension of events or excluding the time window of transient emissions under investigation. For the case of diffuse flux analyses the analysis is optimized on a low energy sample, where the signal is expected to be negligible.

¹ <http://icecube.wisc.edu>

² Atmospheric muons make it impossible to use the Southern hemisphere for ν_μ searches. Cascade analyses can, however, be done for both hemispheres. These results will not be discussed here, but can be found in e.g. [5]

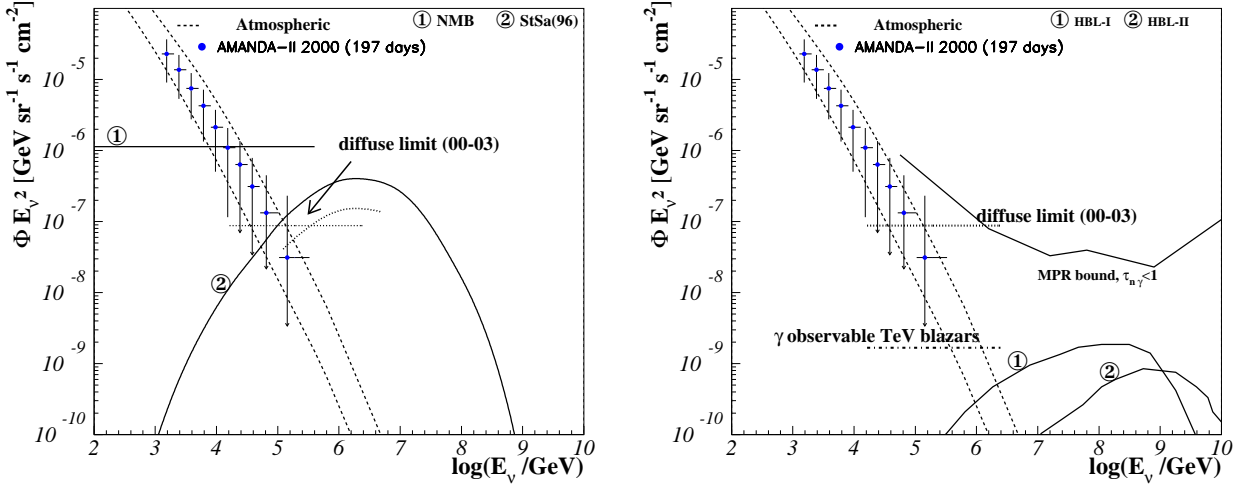


Figure 4. ν spectra for models of ν emission from X-ray emitting AGN (left panel) and for optically thin sources - the cosmic ray flux at the highest energies is assumed to be proportional to the ν output (right panel). Data points are measurements of the diffuse spectrum by AMANDA, year 2000 [8]. Dashed lines represent the atmospheric contribution, the lower line is the vertical flux, the upper one represents the horizontal flux. Limits for 4 years ('00-'03, lifetime=807 days), dotted lines. AGN ν predictions: (1) from Ref. [2]; (2) from [1] (left panel) and (1) and (2) from Ref. [4] (right panel). On the right, the maximum contribution of γ observable blazars is shown as the dot-dashed line. Flux predictions account for ν oscillations.

AMANDA has a twofold strategy for searching for steady point sources. In a first method, a source catalog of 32 sources was established and spatial cuts were determined based on the position of the potential neutrino emitters. The second technique searches for the spatial clustering of events. Neither of the two point source searches has shown a significant excess of events. The mean sensitivity in the Northern hemisphere to an E^{-2} neutrino flux is

$$E^2 \Phi_{lim} = 5.9 \cdot 10^{-8} \text{ GeV cm}^{-2} \text{ s}^{-1} \quad (1)$$

for 5 years of data taking. Here, E is the neutrino energy and Φ_{lim} is the flux upper limit.

The search for single point sources was complemented by stacking classes of sources according to the direct correlation between the photon output and the potential neutrino signal. This was done for 11 different AGN samples that were selected at different wavelength bands, see [6]. The optimum sensitivity was typically achieved by the stacking of around 10 sources. The cumulative and mean source limit for every class is given in table 2.

In the diffuse analysis high-energy (HE) events from all directions are examined with respect to the spectral energy behavior of the sample. A flattening of the total neutrino spectrum is expected when a flat, astrophysical component ($\Phi \sim E^{-2}$) overcomes the steep atmospheric background ($\Phi \sim E^{-3.7}$). The reconstructed energy spectrum for one year of data (year 2000) is shown in Fig. 4. It follows the atmospheric prediction (dashed lines). The most restrictive limit from the diffuse analysis for the years 2000 to 2003 is given as

$$E^2 \Phi_{lim} = 8.8 \cdot 10^{-8} \text{ GeV cm}^{-2} \text{ s}^{-1} \text{ sr}^{-1} \quad (2)$$

in the energy range of $4.2 < \log(E/\text{GeV}) < 6.4$.

The results were obtained by optimizing the analysis cuts on E^{-2} spectra. Nonetheless the dependency of the response function of the detector to different spectra was considered and limits were set for different spectral shapes (e.g. E^{-3}) or specific models as shown in Fig. 4. Varying the spectral index in the simulation shows that the event distribution simulated for AMANDA peaks at very different energies

Table 2. Results of the stacking analysis for each AGN category [7]: the number of included sources N_{src} , the number of expected events N_{ν}^{bg} and the number of observed events N_{ν}^{obs} are listed as well as the cumulative limit f_{lim} as well as the limit per source f_{lim}/N_{source} , both in units of $\text{GeV cm}^{-2} \text{s}^{-1}$.

AGN category	N_{src}	N_{ν}^{obs}	N_{ν}^{bg}	f_{lim}	f_{lim}/N_{src}
GeV blazars	8	17	25.7	2.71	0.34
unidentified GeV sources	22	75	77.5	31.7	0.75
IR blazars	11	40	43.0	10.6	0.96
keV blazars (HEAO-A)	3	9	14.0	3.55	1.18
keV blazars (ROSAT)	8	31	33.4	9.71	1.2
TeV blazars	5	19	23.6	5.53	1.11
GPS and CSS	8	24	29.5	5.94	0.74
FR-I galaxies	1	3	3.1	4.11	4.11
FR-I without M87	17	40	57.2	2.91	0.17
FR-II galaxies	17	77	68.5	30.4	1.79
radio-weak quasars	11	35	41.6	6.70	0.61

depending on the assumed spectral index. While, for an E^{-2} spectrum, 90% of the signal lies between $4.2 < \log(E/\text{GeV}) < 6.4$ as discussed above, an E^{-3} spectrum shows an event distribution located about an order of magnitude lower in energy while an E^{-1} spectrum shifts the sensitivity to higher energies. This shows that it is useful to model the spectra according to the predicted shape. This is discussed in detail in [8].

3. Interpretation of AMANDA diffuse limit

Two main astrophysical implications to be drawn from the current diffuse limit will be examined here. The first is the apparent overproduction of neutrinos in coincidence with X-ray photons in the case of hadronic acceleration at the foot of AGN jets. The second is the maximum contribution of TeV observable blazars to the total diffuse neutrino flux. For a detailed discussion of these and further implications, see [9].

3.1. X-ray/Neutrino correlation in AGN

The left panel of Fig. 4 shows that two models, predicting neutrino emission from X-ray emitting AGN, violate the AMANDA limit. In the case of model 1 [2], the E^{-2} -shaped limit applies (constant, dotted curve), while the limit has been calculated according to the specific shape of the model in the case of model 2 [1] (curved, dotted line). Another model [10] relating neutrino to X-ray emission can be ruled out in the same way. This suggests that the observed X-rays are related to Inverse Compton Scattering rather than to a hadronic scenario. This, however, does not rule out neutrino emission in coincidence with other wavelength bands, like MeV, GeV or TeV sources, for example.

3.2. TeV blazars and Neutrinos

The diffuse neutrino flux from TeV blazars must be lower than the diffuse AMANDA limit:

$$E^2 \frac{dN}{dE} \Big|_{TeV} < 8.8 \cdot 10^{-8} \text{GeV cm}^{-2} \text{s}^{-1} \text{sr}^{-1}. \quad (3)$$

Since TeV photons are absorbed on their way to Earth, current TeV Air Cherenkov telescopes can only detect sources up to $z < 0.3$. TeV photons are believed to be directly correlated to HE neutrinos, since both are produced via the pions from the Δ -resonance resulting from $p\gamma$ interactions. Thus, the detected

neutrino flux from *TeV observable sources* is

$$E^2 \frac{dN}{dE} \Big|_{TeV_{obs}} < 8.8 \cdot 10^{-8} \cdot \eta^{-1} \text{GeV cm}^{-2} \text{s}^{-1} \text{sr}^{-1}. \quad (4)$$

Here, η is the absorption factor, depending on the Star Formation Rate (SFR) scenario and on the maximum redshift, i.e. $z_{\max} = 0.3$. Using a constant density of sources, η is maximized and a limit of $\eta(z_{\max} = 0.3) > 53$ is given. Thus, the upper limit of the contribution of TeV observable sources to a diffuse neutrino flux is given as

$$E^2 \frac{dN}{dE} \Big|_{TeV_{obs}} < 1.7 \cdot 10^{-9} \text{GeV cm}^{-2} \text{s}^{-1} \text{sr}^{-1}, \quad (5)$$

displayed as the dot-dashed line in the right panel of Fig. 4. This underlines the necessity of a diffuse search with HE neutrino telescopes and the need for source-catalog independent searches.

4. Conclusions

Currently, AMANDA is the most sensitive neutrino telescope at high energies. Limits from 5 years for the point source analysis and four years for the diffuse analysis can already be used to constrain the physics of X-ray emission in AGN. Other acceleration mechanisms, predicting the emission of neutrinos in coincidence with TeV, GeV or MeV photons, are still very interesting to look for and represent interesting targets for observation. Optically thin sources are only observable in TeV photons up to $z < 0.3$, which leaves neutrinos as a unique messenger from higher redshifts. IceCube is currently being built at the South Pole as AMANDA's 1km³-successor and the sensitivity will reach levels of $E^2 \Phi_{sens} \sim (2 - 7) \cdot 10^{-9} \text{GeV cm}^{-2} \text{s}^{-1} \text{sr}^{-1}$ in only one year of full observation, see e.g. [11, 12]. This will allow to constrain further neutrino emissions from extragalactic sources, such as AGN and Gamma Ray Bursts (GRBs), or galactic sources such as micro-quasars and Supernova Remnants.

Acknowledgments

Acknowledgments from the IceCube collaboration can be found at <http://icecube.wisc.edu>. The author thanks the BMBF for the possibility to attend the conference (grant: 05 CI5PE1/0).

References

- [1] Stecker F W and Salamon M H 1996 *Space Science Reviews* **75** 341
- [2] Nellen L, Mannheim K and Biermann P L 1993 *Phys. Rev. D* **47** 5270
- [3] Mannheim K, Protheroe R J and Rachen J P 2001 *Phys. Rev. D* **63** 23003
- [4] Mücke A et al. 2003 *Astrop. Phys.* **18** 593
- [5] IceCube Collaboration, contributions to ICRC 2005, Pune (India), *astro-ph/0509330*
- [6] Ackermann et al. 2006, "On the selection of...", accepted for publication in *Astrop. Phys.*
- [7] Achterberg et al. 2006, to be submitted to *Phys. Rev. D*
- [8] Hodges J for the IceCube Collaboration 2006, these proceedings
- [9] Becker J K, Rhode W, Biermann P L Münich K 2006 *astro-ph/0607427*
- [10] Alvarez-Muñiz J and Mészáros P 2004 *Phys. Rev. D* **70** 12, 123001
- [11] Hanson K for the IceCube collaboration 2006, these proceedings
- [12] Halzen F 2006, proc. of "The multimessenger approach to high-energy γ -ray sources", Barcelona (Spain)

Tau Neutrinos in IceCube

D.F. Cowen for the IceCube Collaboration

Physics Department, 104 Davey Laboratory, Pennsylvania State University, University Park, PA 16802 USA

Abstract. Tau neutrino detection in IceCube would be strong evidence for the presence of cosmologically-produced neutrinos. In addition to the well-known “double bang” signature, we describe here five additional channels that we believe will not only extend the energy range over which IceCube can be sensitive to tau neutrinos, but also provide useful control over systematic uncertainties via self-consistency checks amongst all detection channels.

1. Introduction

In the search for ultrahigh energy neutrinos of cosmological origin, few pieces of evidence would be more convincing than a cleanly identified high energy tau neutrino. Tau neutrinos are not produced in standard cosmic-ray atmospheric interactions that create electron and muon neutrinos, and they are expected at immeasurably small levels in the prompt neutrino flux created in charm particle decays in cosmic-ray interactions at high energies [1]. Furthermore, at the energy and distance scales relevant for IceCube detection of atmospheric neutrinos, oscillations of ν_e and ν_μ into ν_τ will be very limited and will not result in large numbers of ν_τ ’s at the detector. After ruling out all these possible high energy ν_τ sources, the only one left is a cosmological source that produces ν_e and ν_μ that oscillate over large travel distances to produce a measurable number of ν_τ ’s at the detector.

The standard UHE neutrino production mechanism is charged pion (and kaon) decay. Pion decay makes a neutrino beam with a flavor ratio of $\nu_e : \nu_\mu : \nu_\tau = 1 : 2 : 0$. It is expected that neutrino oscillations will result in a 1:1:1 flavor ratio at the detector, and large deviations from this ratio would be an indication of new or unexpected physics, either in the production mechanism at the source, the propagation of the neutrinos over cosmological distances, or in the neutrino oscillation mechanism itself [2]. Likewise, excessive ν_τ ’s at atmospheric neutrino energies might also be an indicator of new physics, but IceCube will have limited ability to exclusively identify ν_τ ’s at these lower energy scales, where a cascade from a ν_τ will be very difficult to distinguish from a cascade from a charged-current ν_e , a neutral-current any-flavor neutrino, or a low energy charged-current ν_μ interaction.

2. Tau Neutrino Signatures in IceCube

By virtue of the tau lepton’s long decay length at ultrahigh energies, and its wide variety of decay modes, a tau produced in a charged-current ν_τ interaction has a rich set of possible signatures in the IceCube detector. The tau decay length is about 50 m per PeV, so a tau with E_τ up to about 20 PeV can be fully contained in the detector volume. More generally, the tau production vertex, decay vertex or both may be observable in a single event. The tau can decay leptonically, $\tau \rightarrow e\nu_e\nu_\tau$ (branching ratio = $\sim 18\%$) or $\tau \rightarrow \mu\nu_\mu\nu_\tau$ ($\sim 18\%$), or hadronically, mainly to charged and neutral pions and kaons ($\sim 64\%$). Note that since the average charged-current ν_τ interaction produces a tau with $0.75E_\nu$, we will assume $E_\nu = E_\tau$ and refer to either as just “E” for the sake of simplicity.

The following subsections and Figure 1 list six tau neutrino signatures to which IceCube may be sensitive. For each signature we also describe the chief expected backgrounds, energy range over which

IceCube will have sensitivity, relevant tau branching ratio, rough IceCube angular acceptance, and energy and pointing resolution relative to that expected for ν_e and ν_μ events. In order to assure that we can distinguish a tau track from one or both of its cascades, or from a muon track, we require a tau track length of at least 200 m in the detector. However, energetic downward-going taus will encounter a higher number of DOMs (Digital Optical Modules) [3] per unit track length, decreasing the minimum required track length and hence the energy threshold. Likewise, some taus will simply live longer, also lowering the energy threshold somewhat. Detailed Monte Carlo studies of IceCube sensitivity versus track length will change our simplistically sharp 200 m cutoff.

2.1. Double Bang

The classic ν_τ signature is the “double bang” in which the initial charged-current interaction creates a hadronic shower and a tau lepton [4]. The tau lepton has sufficient energy to travel a long enough distance in the detector such that when it decays ($\tau \rightarrow e\nu_e\nu_\tau$ or $\tau \rightarrow$ hadrons ν_τ , total BR = $\sim 82\%$), it produces a second, separately visible shower. The tau lepton connecting the two showers will also emit Cherenkov light. Depending on the length of the tau track, and the extent to which the two showers are contained, IceCube can get the best of both worlds when reconstructing such an event: the pointing resolution can be comparable to that of ν_μ , and the energy resolution to that of ν_e . IceCube should have slightly more than 2π sr acceptance in this channel, since upward-going ν_τ ’s are either absorbed or degraded in energy by passage through the earth. There should be negligible background, although in principle downward-going signal events could be faked by coincident muons from cosmic-ray air showers. The fake rate is probably too small to be a concern, but Monte Carlo studies are needed to verify this. The requirements that the two showers are well-separated (more than ~ 100 m apart) and contained give a ν_τ energy acceptance range of $E \sim 2\text{-}20$ PeV.

2.2. Lollipop

If the tau lepton is created sufficiently far from the fiducial volume that the initial hadronic shower is not visible by the detector, and the tau then enters the fiducial volume and decays to produce a shower (total BR = $\sim 82\%$), the event signature resembles a lollipop: a track ending in a shower. The pointing resolution of lollipop events should be comparable to that of ν_μ , while the energy resolution will be better but not as good as for ν_e on account of the missed initial shower. Requiring that the tau have at least 200 m of length in the fiducial volume gives an energy acceptance range of $E \gtrsim 5$ PeV. At this energy scale we are restricted to $\sim 2\pi$ sr acceptance since upward-going neutrinos are either absorbed or degraded in energy by passage through the earth. This channel may be sensitive to background from coincident muons from cosmic-ray air showers. Again, this background rate would need to be estimated from Monte Carlo.

2.3. Inverted Lollipop

If the tau lepton is instead created inside the fiducial volume and then decays undetectably outside the volume, the signature also resembles a lollipop, but created in inverse order (shower first, track second). While there is no branching ratio factor here—100% of the ν_τ that experience a charged-current interaction in the detector volume will produce a tau in the detector volume—and while the pointing and energy resolutions are comparable to that of the non-inverted lollipop, the inverted lollipop is susceptible to an irreducible background from ν_μ charged-current events. (A ν_μ can have a charged-current interaction in the fiducial volume, creating a shower and a muon, the combination of which will be very hard to distinguish on an event-by-event basis from ν_τ inverted lollipops. Of course, the event itself is still of interest, especially if its energy is high enough to make it a candidate for being of cosmological origin, but here we are concerned mainly with events that we can convincingly identify as coming from a ν_τ .) This channel is also susceptible to background from cosmic-ray muons accompanied by a bremsstrahlung interaction, a background that may be studied (but not eliminated) using an IceTop-tagged muon beam in the data. As with the lollipop signature, requiring that the tau have at least 200 m of length in the fiducial volume gives a energy acceptance range of $E \gtrsim 5$ PeV. As in the double bang and lollipop channels above, this energy scale also restricts this channel to $\sim 2\pi$ sr acceptance.

2.4. *Sugardaddy*

If a tau is created well outside the fiducial volume, then enters it and decays to a muon rather than a shower inside the volume (BR = $\sim 18\%$), it creates a unique signature which may be detectable. As described in Ref. [5], the much heavier tau will emit significantly less light along its length compared to its lighter daughter muon. This can be idealized as a step-function change in track brightness. For energies between roughly 1 PeV and 1 EeV, the magnitude of the change is expected to be larger than the track energy resolution of IceCube, and hence it should be detectable. There is no background aside from the very unlikely high energy muon that by random chance has significantly more stochastic light-producing interactions at later times relative to earlier times along its length.³ The energy resolution should be comparable to that of a standard ν_μ event. Requiring at least 200 m of tau track in the fiducial volume sets the energy scale for these events at $E > 5$ PeV.

2.5. *Double Pulse*

At energies below the scale at which the two showers of a double bang can be resolved as two separate cascades by the full detector, there is an energy range in which one or more DOMs near the two closely-spaced showers will see a double-peaked structure in its waveform. The lower end of the energy acceptance range for this signature is defined by the ability of a DOM to resolve two waveforms. We assume here that the two waveforms need to be separated in time by ~ 20 ns, from which we infer a lower energy of ~ 100 TeV, corresponding to roughly a 5 m tau decay length. Assuming the popular E^{-2} spectral shape of the neutrino signal flux, this order-of-magnitude improvement in energy sensitivity relative to the standard double bang signature may be a great benefit, even after taking into account the phase space factor reduction in acceptance due to the need for favorable spacing and orientation of the two showers relative to the DOM(s). Note that there will be slivers of phase space where the tau direction is highly favorable for creating resolvable waveforms, possibly decreasing the lower end of the energy acceptance range by an additional factor of 2 to 3. Monte Carlo studies are underway to map out this phase space in energy and tau orientation. The chief background to this signal would come from two successive bremsstrahlung interactions in a downward-going cosmic-ray muon event. Presumably this background can be addressed simply by removing events with track-like topologies and requiring that all events are well contained within the fiducial volume.

2.6. *Tautsie Pop*

When a tau is at such low energy that its production and decay vertices are indistinguishable in IceCube, the decay $\tau \rightarrow \mu\nu_\mu\nu_\tau$ will produce an inverted-lollipop-like signature in the detector and may give us access to very low tau neutrino energies. The additional two neutrinos in the tau decay are the key difference between this signal and its backgrounds from, for example, charged-current ν_μ interactions. These neutrinos will carry away energy, causing the ratio $E_{\text{shower}}/E_{\text{track}}$ to be larger by a factor of 2 to 3 in tau events than in background events. Due to event-to-event variations in $E_{\text{shower}}/E_{\text{track}}$, and due to the relatively small ratio difference factor, this analysis would have to be done on a statistical basis. Although this channel suffers from the 18% $\tau \rightarrow \mu\nu_\mu\nu_\tau$ branching ratio, it benefits from its reach to very low energies, starting at roughly where the “double pulse” topology leaves off and extending down to energies perhaps as low as tens of TeV. The lower bound is determined by the energy at which the emerging muon track travels too short a distance to get a good handle on its energy, although ideally one could get to very low muon energies using events in which the muon decays in the detector volume. At low enough energies, tau neutrinos from atmospheric interactions may start entering as a “background” to cosmological tau neutrinos. In principle, background from cosmic-ray muons that have a fortuitous bremsstrahlung interaction could be estimated from a sample of IceTop-tagged muons in the data. Background from charged-current ν_μ interactions would have to be estimated from Monte Carlo.

³ This potential background may be conservatively estimated from data by measuring the probability for tracks to have a step-function-like change in brightness but in the opposite sense from that expected for tau decays, i.e., brighter then dimmer.

3. Conclusion

Figure 5 summarizes the tau decay channels that may be accessible to IceCube. In addition to the canonical double bang channel, five other channels may also be detectable. The energy range is extended considerably beyond that available from just the double bang channel alone, and in many cases the overlapping energy ranges will permit IceCube to make simultaneous tau neutrino flux measurements using channels with very different systematics.

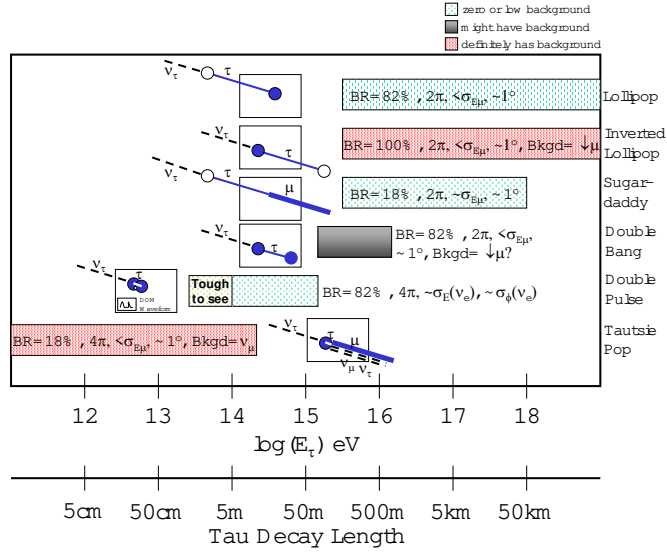


Figure 5. Summary of τ channels possibly accessible to IceCube, shown as a function of energy and approximate tau decay length, with indications of background level, acceptance, angular and energy resolutions, and specific anticipated background.

References

- [1] M. Thunman, G. Ingelman and P. Gondolo, Astropart. Phys. **5**, 309 (1996) [arXiv:hep-ph/9505417]; L. Pasquali and M.H. Reno, Phys. Rev. D **59**, 093003 (1999) [arXiv:hep-ph/9811268]; J.F. Beacom and J. Candia, JCAP 0411, 009 (2004) [arXiv:hep-ph/0409046]; S.I. Dutta, M.H. Reno and I. Sarcevic, Phys. Rev. D **62**, 123001 (2000) [arXiv:hep-ph/0005310]; H. Athar, K.M. Cheung, G.L. Lin and J.J. Tseng, Astropart. Phys. **18**, 581 (2003) [arXiv:hep-ph/0112222]; A.D. Martin, M.G. Ryskin and A.M. Stasto, Acta Phys. Polon. B **34**, 3273 (2003) [arXiv:hep-ph/0302140].
- [2] Kashti and Waxman, astro-ph/0507599 and Barenboim and Quigg, hep-ph/0301220.
- [3] IceCube Collaboration, Astropart. Phys. **26**, pp. 155-230 (2006).
- [4] J.G. Learned and S. Pakvasa, Astropart. Physics J. **3**, p. 267 (1995).
- [5] T. De Young, S. Razzaque and D. Cowen, arXiv: astro-ph/0608486.

IceCube: Multiwavelength Search for Neutrinos from Transient Point Sources

Elisa Resconi for the IceCube Collaboration

Max-Planck-Institute for Nuclear Physics, Saupfercheckweg 1, 69117 Heidelberg, Germany.

E-mail: elisa.resconi@mpi-hd.mpg.de

Abstract. In this paper we discuss the strategy developed in order to associate neutrinos with their cosmic sources using historical light curves. Periods of very intense photon activity are selected through a novel analysis approach. The statistical method called *Maximum Likelihood Blocks* is applied for the first time on light curves of high frequency blazars. In order to avoid any possible bias in the selection of periods with intense photon activity, the arrival time and incoming direction of the neutrinos are kept blinded. Following the approach here reported, neutrino fluxes below the atmospheric neutrino background level can become accessible. We report as well on a first step to establish a target-of-opportunity program based on neutrinos detected in IceCube which are used as alerting messenger particles.

1. Introduction

We report here on the inclusion of the photon flux time evolution, measured in one or more photon wavebands, in the search for HE neutrino sources. We illustrate this approach by a discussion of blazars. In the framework of *hadronic models* [5, 6], blazars are HE neutrino sources and they are dominated by a highly variable component of non-thermal radiation [3]. Blazar broad-band spectra consist of two prevalent components which appear in the spectral energy distribution like two broad humps. The low-energy component can peak at various frequencies between optical and X-ray and the high-energy is proportionately shifted from X-rays up to very high energy (VHE) γ -rays. The synchrotron radiation coming from primary electrons as well as from electrons produced in proton-induced cascades contributes to the low-energy component. In hadronic models, high-energy radiation arises from photo-meson interaction and from proton and muon synchrotron radiation [6]. The γ -ray production by pion photo-production is accompanied by neutrinos, created in the decay of charged pions.

So, assuming that neutrino production follows the same time behaviour like the electromagnetic activity, the transient nature of the energetic emission can be used to improve the association between highly energetic neutrinos and non-thermal sources. If the enhancement of the neutrino signal is concentrated in a short period of time, neutrino flares not evident in a time-integrated point source search like the one reported in [1], might be detectable. A first analysis following this approach has been discussed in [7, 8]. In this paper, we concentrate on the statistical interpretation of measured light curves.

2. Collection and Interpretation of Light Curves: Periods Selection

IceCube Collaboration has started a comprehensive collection of historical light curves. For now, most of our efforts are concentrated on X- and VHE γ -ray wavebands which corresponds to the two humps of the spectral energy distribution for high frequency blazar (HBL). The two instruments used for X-ray data are All-Sky Monitor (ASM) [9] and the Proportional Counter Array (PCA) installed on board of

the Rossi X-ray Timing Explorer (RXTE). RXTE standard data products are collected directly from the HEASARC database and then transformed in *root* format. A large set of data has been collected by VHE γ -ray experiments [10]. Moreover, optical data has been as well taken for few sources and reported in [11].

In order to utilize the transient character of the electromagnetic emission for HE neutrino search, we have first to separate variable periods (*flares*) and steady state periods of a source. Periods of no variable activity are often defined in the literature as *quiescent* but an apparent *quiescent* level can be due to a superposition of numerous unresolved flares or to a limited sensitivity of the instrument [14]. We call the level of activity in which the source stays for the longest period of time its *characteristic* level. We do not attempt to interpret this level in phenomenological terms. Often data are affected by large uncertainties or the data spacing is rather inhomogeneous. In order to improve the interpretation of photon data, a simple and model-independent approach has been applied. The method aims at dividing the light curves in time intervals in which the source emission is compatible with a constant level. An algorithm based on Bayesian statistics that provides such a segmentation of data of different nature was presented in [13] and a modified version based on Maximum Likelihood was recently employed in studies of stellar X-ray light curves [14]. We will refer to this algorithm as the method of Maximum Likelihood Blocks (MLBs); its first application to blazars X- and VHE γ -ray light curves has been reported in [15].

The MLBs sub-divides the light curve into constant-flux intervals or *blocks*. The confidence level at which the algorithm splits the light curve is given as input to the algorithm (in this work 99%). From this interpretation of the data we can extract various information about the source like the time a source pass in a particular activity state, if there are favorite flux levels and the periods in which the source is in *flare* state. For a visualization, the flux value of the single block is histogrammed and the duration of the block is used as a weight for the single entry. In Fig. 6, the histogram of ASM blocks are reported for the Mkn421 as example. The peak of the distribution is quite naturally interpreted as the *characteristic* level. The tail at higher flux values represent the flaring activity of the source; the tail at negative flux indicates measurement errors in the ASM data. Mean value and the standard deviation of a fitted Gaussian are then interpreted as the *characteristic* level R_{char} and σ_{char} , respectively. An example of such interpretation is shown in Fig. 7. With this interpretation of the light curve, the periods of time when the source is in *flare* can be selected requiring that the photon flux deviates from the characteristic level for a certain number of standard deviations. In this way, a uniform selection of *flares* is obtained on years-long light curves. A similar procedure applied on VHE data failed in the identification of a possible VHE γ -ray characteristic level. Nevertheless, an arbitrary flux threshold can be placed in order to select flaring periods on VHE light curves. Considerations about the VHE data are reported also in [10, 11].

A comparison of the time behaviour of different wave length bands may lead to a particularly interesting classification of periods for the neutrino search, as will be described below. Nearly simultaneous X- and VHE γ -ray data are collected from organized multi-wavelength campaigns. The time and flux correlation between the X- and γ -ray components have been investigated [12]. In most of the cases, a time-correlation between the two components has been observed as expected in the framework of *leptonic models*. So called orphan flares, where an increasing TeV flux is not accompanied by an increase of the X-ray flux, have been seen in at least two sources: 1ES 1959+650 and Mkn 421. A study of the correlation between these two wavebands using the high statistic light curves collected is under way and results will be reported elsewhere.

3. Toward a Multi-messenger Approach

The use of historical light curve to improve the search for HE neutrino sources is limited by the low duty cycle of γ -ray telescopes and rare long term observations. Neutrino telescopes, on the contrary, like IceCube are characterized by a very wide field of view and very high duty cycle. HE neutrinos are produced exclusively by hadronic mechanisms and are expected to be time-correlated with the related photon emission. In order to improve the synchronous measurement of both photons and neutrinos, the idea to develop a *hadronic* trigger or target of opportunity (ToO) using HE neutrino candidates has been born within the IceCube Collaboration [8]. The ToO under discussion concerns transient phenomena of particularly interesting targets, as well as unpredictable sudden astronomical events. HE neutrino

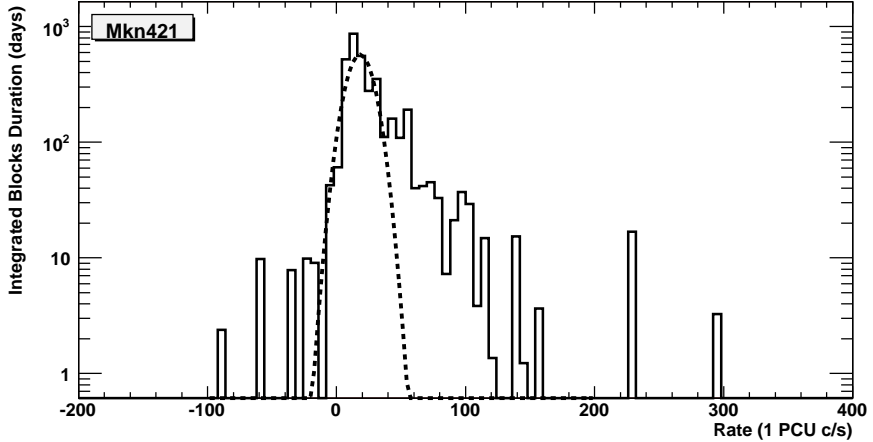


Figure 6. Duration of maximum likelihood blocks for Mkn421, based on ASM flux. This represents the measurement of the integrated time a source stays at a given flux level. In particular, the flux of the peak is the flux level in which the source stays for the longest time and therefore corresponds to the characteristic level. Negative blocks are due to systematic errors in ASM.

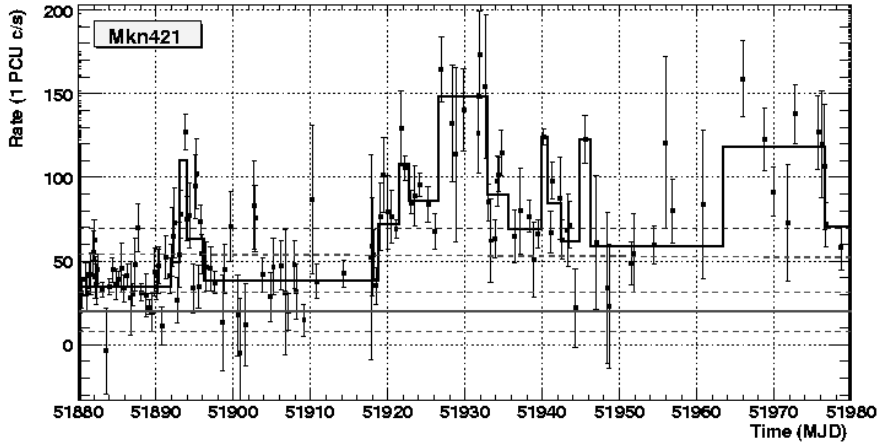


Figure 7. Mkn421, sub-period of 100 days of ASM light curve (10 years total time of observation), blocks (99% C.L.). The continuous red line corresponds to the *characteristic level* R_{char} , the dotted line represent $1\sigma_{char}$ and $3\sigma_{char}$ deviation from R_{char} . The blue line corresponds to $R_{char} + 5\sigma_{char}$. The X-ray units are normalized to 1 PCU count/second (1 Crab ≈ 3000 counts/sec/detector).

candidates are reconstructed on-line at the South Pole as up-going muon tracks. Information on these events can be transferred north via satellite and, in principle, be used as the alert messengers for other telescopes. The technical realization of such alerts is under investigation and results are encouraging. The first telescope already reacting to neutrino ToO program is the MAGIC VHE γ -ray telescope. A test run started on September 27 (2006) is based on AMANDA data acquisition system and will last for a few months. The test is focused on technical aspects, such as the recording and real time reconstruction of

the neutrinos at the South Pole, the reception of the triggers by MAGIC and the communication between the two instruments.

To date, no indication of HE cosmic neutrinos has been found in the performed analysis of AMANDA data. Contrary to other ToO programs, the alert in the case of the neutrino ToO is issued on the basis of a non clear detection. Non-trivial statistical issues related to the interpretation of possible coincidences are under careful investigation and will be reported elsewhere. Beyond that, once a significant accumulation of HE neutrinos will be observed in IceCube, the simultaneous photon data provided by ToO programs will lead to a mature phenomenological picture of the astronomical object observed.

References

- [1] Ackermann M et al 2006 Proceeding of The Multi-Messenger Approach to High Energy Gamma-ray Sources, Barcelona, to be published in Astrophysics and Space Science Manuscript
- [2] Achternberg A et al 2006 On the selection of AGN neutrino source candidates for a source stacking analysis with neutrino telescopes *Preprint astro-ph/0609534*
- [3] Begelman M C, Blandford R D, Rees M J 1984 *Rev. Mod. Phys.* 56, 255
- [4] Jones, O'Dell, Stein, 1974 *ApJ* 188, 353
Mastichiadis, Kirk J 1997 *A&A*, 320, 19
- [5] Mannheim K 1993 *A&A* 269, 67
- [6] Mücke A., Protheroe R J 2001 *Astroparticle Physics* 15, 121-136
Aharonian F A 2002 *MNRAS* 215A, 332
- [7] Ackermann M et al 2005, Proceeding of 29th International Cosmic Ray Conference (ICRC 2005) Pune (India) *Preprint astro-ph/0509330*, 24-27
- [8] Bernardini E et al 2005, Proceeding of 7th Workshop of Towards a Network of Atmospheric Cherenkov Detectors 2005, Palaiseau, France *Preprint astro-ph/0509396*
- [9] Levine A M et al 1996 *The Astrophysical Journal*, 469, L33-L36
- [10] Tluczykont M, Shayduk M, Kalekin O, Bernardini E, Long-term Gamma-Ray lightcurves and high-state probabilities of Active Galactic Nuclei, these Proceedings
- [11] Bayer M, Larson K, Montaruli T, Steele D, Joint Multi-Wavelength Observations of Blazars with WIYN-VERITAS-IceCubeType, these Proceedings
- [12] Krawczynski H, Coppi P S, Maccarone T, Aharonian F A 2000 *A&A* 353, 97
Krawczynski H et al 2004 *ApJ* 601, 151
- [13] Scargle J D 1998 *ApJ* 504, 405
- [14] Wolk S J et al 2005 *Astophys.J.Suppl* 160, 423
- [15] Resconi E, Gross A, Costamante L, Flaccomio E, Franco D, icecube/200608002

Air showers in a three dimensional array: Recent data from IceCube/IceTop ⁴

Xinhua Bai & Thomas K. Gaisser for the IceCube Collaboration

Bartol Research Institute and Department of Physics and Astronomy
University of Delaware, Newark, DE 19716 USA

E-mail: bai@bartol.udel.edu, tgaisser@bartol.udel.edu

Abstract. The next generation high energy neutrino and cosmic ray array IceCube/IceTop is under construction at the geographic South-Pole. Air showers with trajectories that pass through the surface array and near the deep strings trigger both components in coincidence. The ratio of the muon signal in the deep detectors to the shower signal on the surface is sensitive to the elemental composition of the primary cosmic radiation.

One string of 60 sensors buried between 1.5 and 2.5 km in the ice and a surface array of 4 stations were successfully deployed at the South Pole during the austral summer of 2004-05 and have been producing data since February 2005 [1]. Eight more strings and 12 more IceTop stations were deployed in the austral summer of 2005-06. Since then 16 stations and 9 strings have been operating. The full array with up to 80 strings and 80 surface stations is scheduled for completion in 2011.

Each IceTop station consists of a pair of ice Cherenkov tanks (to be referred to as tank A and B) separated by 10 m, each containing a cylinder of clear ice $2.7 \text{ m}^2 \times 0.9 \text{ m}$ viewed from the top by two standard IceCube digital optical modules (DOMs). The operation of a surface array over the deep IceCube neutrino telescope has three goals:

- Composition: To study the ratio of the muon signal in the deep array to the shower signal on the surface which is sensitive to the fraction of heavy nuclei in the cosmic-ray spectrum.
- Calibration: To study the angular resolution and pointing accuracy of the neutrino array by providing a sample of externally identified muon bundles.
- Filtering: To study and filter single or multiple muon background in the deep detector by tagging the associated air-shower activities on the surface.

Predecessors for operation of a surface array in conjunction with a deep underground detector sensitive to muons are SPASE-AMANDA [2] and EASTOP-MACRO [3]. With an acceptance at completion of $\sim 0.3 \text{ km}^2 \text{sr}$, IceTop/IceCube will have a significantly higher reach in primary energy than these earlier experiments. With a threshold of approximately 300 TeV, the experiment will be sensitive from below the knee of the cosmic-ray spectrum up to approximately 1 EeV, where it will be statistically limited by its acceptance. A significant motivation for studying the composition in this energy region is to search for the transition from a population of cosmic rays primarily of local origin in the Milky Way Galaxy to a population of extra-galactic origin [4].

Figure 8 shows the integral energy spectra of muons at production in the atmosphere in proton-initiated showers of various primary energies. The two vertical arrows indicate the minimum muon

⁴ Research supported by the U.S. National Science Foundation

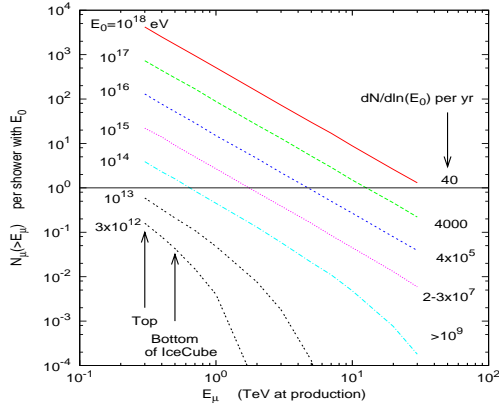


Figure 8. Integral energy spectra of muons in air showers (see text).

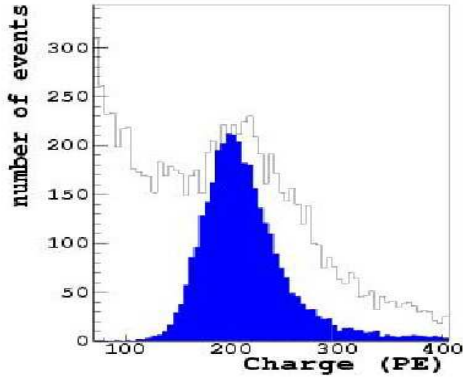


Figure 9. Charge spectrum of pulses in an IceTop tank (see text).

energies needed to reach the top and bottom of the deep in-ice detector. Each spectrum is labeled on the right with the number of coincident events per year ($dN/d\ln E$) expected within the acceptance of the full detector. The currently operating array with 16 surface stations and 9 strings has approximately 0.5% of the geometrical acceptance for coincident events of the full detector and is therefore statistically limited at 10^{17} eV, where the expected number of events per year would be about 20 (as compared to 4000 for the completed detector).

Low-energy atmospheric muons (typically in the GeV range) provide a natural beam for calibrating and monitoring the response of IceTop detectors to track length above Cherenkov threshold and hence to the energy deposition in the tanks. The characteristic spectrum (shown in Fig. 9) combines the steeply falling spectrum of electrons and converting γ -rays with a peak due to muons. Small air-showers contribute to the high-energy tail. The solid histogram in Fig. 9 shows the single muon peak identified by a muon telescope in a special run. The tagged muon histogram is narrower than the muon peak in the composite spectrum and very slightly shifted toward the lower integrated charge. The vertical through going muon deposits 160 MeV and thus provides the conversion between energy deposition and integrated charge of the waveform. Special, periodic monitoring runs obtain the composite, inclusive spectrum to look for any change in shape or peak location, which would indicate a change in tank response.

In normal data taking, the IceCube data acquisition system sends data to the surface only if neighboring DOM pairs are hit. For IceTop, we require that both tanks at the same station register a hit so that only air showers are reported. Events are recorded if the hits satisfy a simple majority trigger (SMT). For IceTop, the SMT is set to 6 DOM hits within $2\mu s$; for in-ice detector, the SMT is set to 8 hits within $5\mu s$. With these settings, the in-ice trigger rate is 146 Hz and the IceTop SMT rate is 7.1 Hz. Whenever either trigger is satisfied, waveforms of all hit DOMs are recorded. Of particular interest is the subset in which both SMT triggers are satisfied. This coincident rate is measured to be 0.19 Hz in the 2006 detector configuration. These events will be the subject of the composition analysis. They also provide tagged muon beams for the calibration of in-ice array.

Figure 10 shows the lateral distribution for a typical large IceTop event, which happens to be a coincident trigger. Figure 11 shows the waveforms on the surface at two locations (~ 100 m and ~ 210 m from the reconstructed shower core) and a sample waveform from an in-ice DOM in the same event. Surface waveforms have the characteristic features of large, smooth shape near the core and smaller, more uneven structure farther out. In-ice waveforms are typically a sequence of single photo-electrons.

Finally, Figs. 12 and 13 illustrate cross calibration of angular resolution between IceTop and the deep-ice array of IceCube. When the realistic curved shower front (dashed in 12) is used, the directions agree well ($FWHM \approx 5^\circ$). A sub-array analysis is in progress to determine the angular resolution of the IceTop reconstruction algorithm. This analysis uses the pairwise distribution of tanks to form one sub-array of all 16 “A” tanks and a second sub-array of all 16 “B” tanks at each station. Comparison of the separately determined “A” and “B” directions for each event give a measure of the resolution of IceTop alone. Deconvolving the distribution of Fig. 13 will then give a measure of the resolution of the in-ice reconstruction algorithm as applied to muon bundles.

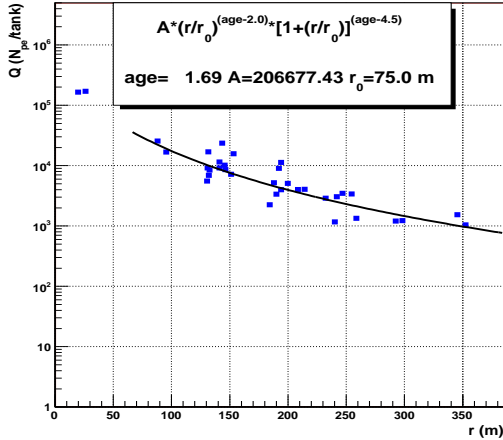


Figure 10. Lateral distribution of the charge in surface tanks fitted with an NKG distribution.

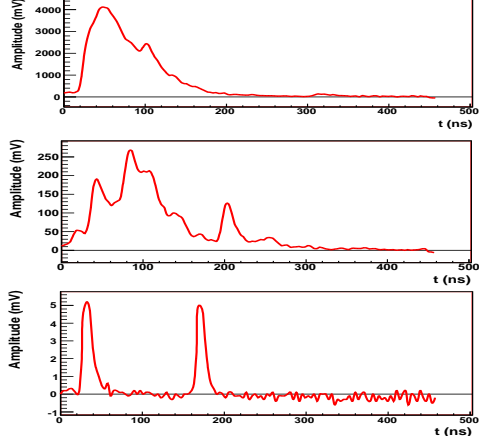


Figure 11. Waveforms in coincident events (see text).

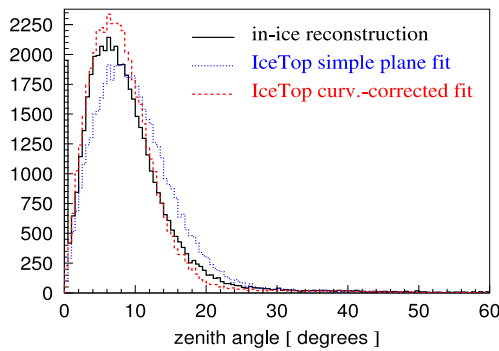


Figure 12. Zenith angle distribution of coincident events as reconstructed by in-ice alone (black histogram) and by IceTop alone with two different procedures.

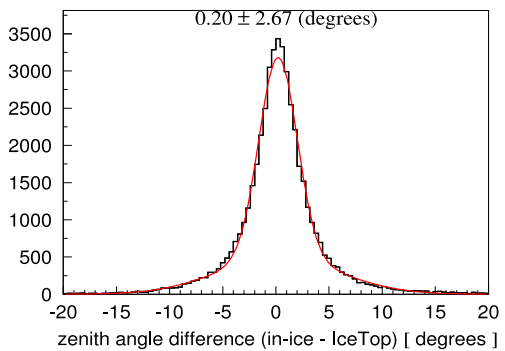


Figure 13. Distribution of the difference between directions determined by IceTop alone and by using the in-ice muon reconstruction algorithm.

- [1] Achterberg A et al. (IceCube Collaboration) 2006 *Astropart. Phys.* **26** 155
- [2] Ahrens J et al. 2004 *Astropart. Phys.* **21** 565
- [3] Aglietta M et al. (EAS-TOP and MACRO Collaborations) 2004 *Astropart. Phys.* **20** 641; 1994 *Phys. Lett.B* **337** 376
- [4] Hillas A M "Cosmic Rays: Recent Progress and some Current Questions" arXiv:astro-ph/0607109

High-Energy Gammas from the giant flare of SGR 1806-20 of December 2004 in AMANDA

Juan-de-Dios Zornoza for the IceCube Collaboration⁵

222 W. Washington Ave. Madison WI 53703 (USA)

E-mail: zornoza@icecube.wisc.edu

Abstract. We show in this paper the analysis of the AMANDA-II data looking for events correlated with the giant flare observed in December 27th 2004 from the Soft Gamma-ray Repeater 1806-20. This flare was more than two orders of magnitude brighter than any previous flare of this kind and saturated the satellite gamma detectors that observed it. If a hard component of gamma-rays was present in the event, these would produce detectable rates of muons in underground detectors like AMANDA. Moreover, high-energy neutrinos could also have been emitted in quantities large enough to produce a signal in this detector. The unblinding of the data showed no signal, so upper limits were set both to the gamma-ray and the neutrino fluxes.

1. Introduction

Soft Gamma-ray Repeaters (SGRs) are X-ray pulsars which emit X-ray bursts lasting ~ 0.1 s during sporadic active periods. The typical luminosities of these bursts is 10^{41} erg/s. However, there are rare occasions in which giant flares (in X-rays and soft-gamma rays) are observed, with luminosities thousands of times higher than normal bursts. Three of these giant flares had been observed until 1998 [1]. On December 27th 2004, a giant flare of soft-gamma rays and hard X-rays coming from the Soft Gamma-ray Repeater 1806-20 saturated several satellite gamma-detectors [2, 3, 4]. This was the brightest transient event ever observed in the Galaxy.

The most accepted theory to describe SGRs is the “magnetar” model. According to this model, these objects are very-rapidly-rotating neutron stars, with extremely high magnetic fields ($B \sim 10^{15}$ G, two orders of magnitude larger than in normal neutron stars). Along time scales of the order of tens of years, these strong magnetic fields build up an increasing stress in the star. When the stress on the star crust is too strong, it fractures. This produces a starquake which liberates enormous quantities of energy in X-rays and γ -rays as the magnetic field rearranges [5].

The energy spectrum of the Dec. 2004 flare can be described as the sum of a black-body spectrum and a power law [6], which would indicate a relevant component of high-energy (\sim TeV) emission. High-energy gammas would produce showers when interacting at the top of the Earth’s atmosphere. These showers would be muon-poor, but some of the many photons produced in these interactions would produce pions. The decay of these pions would yield muons which can reach underground detectors like AMANDA [7].

High-energy neutrino fluxes have been also predicted by some authors [8, 9], if there is a significant baryonic outflow. In this case, neutrinos could also reach underground neutrino detectors and produce a signal.

⁵ <http://www.icecube.wisc.edu>

2. The AMANDA detector

The AMANDA neutrino telescope [10] consists of a three dimensional array of 677 Optical Modules (OMs). An Optical Module is basically a photomultiplier and its electronics housed in pressure-resistant glass sphere. These OMs are distributed along 19 strings buried 1500-2000 m deep in the Antarctic ice.

The main aim of this experiment is the detection of cosmic neutrinos. The principal signature is given by high-energy neutrinos interacting in the surroundings of the detector and producing a relativistic muon which would emit Cherenkov light when traveling in the ice. Events are recorded when at least 24 OMs register a signal within 2 μ s. The information of the position and the time of the photons hitting the photomultipliers is used to reconstruct the direction of the neutrino. As we have mentioned before, the main motivation in this analysis is the search for muons produced indirectly in the showers induced by gamma-rays interacting in the top atmosphere. Since the source was above the horizon, the effective area for TeV photons is one order of magnitude higher than for neutrinos. However, there is no way to distinguish between both possibilities in case of the observation of a muon.

3. Analysis

Since both the time and the position of the burst can be well constrained, the enormous background of muons produced by cosmic rays in the atmosphere can be effectively reduced.

There are two variables to optimize in this analysis: the width of the time window and the angular size of the search cone. In order to prevent a possible bias in the analysis, we perform the optimization of the selection criteria with the data blinded, which is particularly relevant when small signals are expected, as it is our case.

The duration of the burst was \sim 0.6 s. However, this window had to be widened in order to account for the dispersion in the times given by the satellites [11, 12, 2, 4, 13], calculated at the location of the detector. The chosen window, once these facts were taken into account is 1.5 s around UT 21h 30m 26.6s of December 27th.

The next step is to determine the best search cone. This is done by optimizing the so-called Model Discovery Factor (MDF) [14], defined as

$$MDF = \frac{\mu(n_b, CL, SP)}{n_s} \quad (6)$$

where μ is the Poisson mean of the number of signal events which would result in rejection of the background hypothesis, at the chosen confidence level CL , in $SP\%$ of equivalent measurements. n_s and n_b are the number of signal and background events, respectively.

The background was determined using on-source, off-time, real data (the data \pm 10 minutes around the burst is kept blinded). It was also checked that the detector rate on December 27th was stable (rate \sim 90 Hz, close to the AMANDA average).

The signal is simulated in order to estimate the angular resolution and the effective area of the detector. With the codes CORSIKA-QGSJET01 [4] and ANIS [16], we generated photons and neutrinos, respectively, with energies ranging from 10 TeV to 10^5 TeV. The secondary muons are propagated up to the detector and reconstructed.

The dependence of the MDR on the search cone is shown in figure 14 (left). It can be seen in that plot that the optimum size corresponds to a radius of 5.8°. The expected background for such a cone, during 1.5 s is 0.06 events, at the location of the source.

4. Results

Once the optimum selection criteria were found, the data were unblinded. However, no event was found correlated with the burst. Therefore, upper limits were set, based on the effective area of the detector. Assuming a power law spectrum $\frac{dN}{dE} < A_{90}(E/\text{TeV})^\gamma$, the limits on the normalization constant of the flux of gamma-rays and neutrinos are shown in figure 14 (right), as a function of the spectral index. This means, for instance, limits of 0.05 (0.5) $\text{TeV}^{-1} \text{m}^{-2} \text{s}^{-1}$ for $\gamma = -1.47$ (-2) in the gamma flux and 0.4 (6.1) $\text{TeV}^{-1} \text{m}^{-2} \text{s}^{-1}$ for $\gamma = -1.47$ (-2) in the high-energy neutrino flux (at 90% CL).

Acknowledgments

This work has been done with the financial support of the Marie Curie OIF Program.

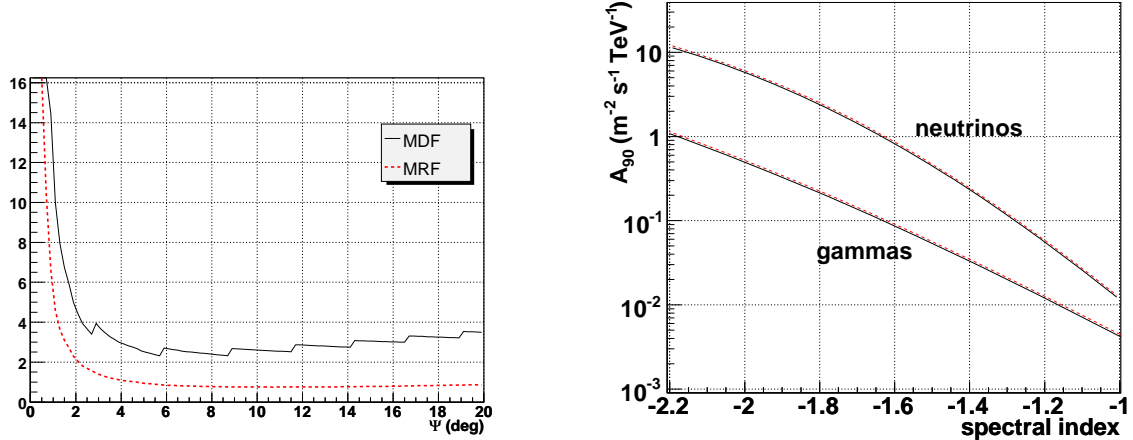


Figure 14. Left: Model Discovery Factor (solid, black) and Model Rejection Factor (dashed, red) as a function of the radius of a circular angular acceptance window, for an $E^{-1.47}$ spectrum. Right: Sensitivity (dashed, red) and limit (solid, black) to the normalization constant in the flux of gammas (lower line) and neutrinos (upper line), as a function of the spectral index, assuming a flux $\phi(E) = A (E/\text{TeV})^\gamma$.

References

- [1] Barat C., et al., *Astron. Astrophys.* **79**, L24-L25 (1979); Cline T., et al. *IAU Circ.* No.7002 (1998)
- [2] Borkowski D. et al., *GCN Circ.* **2920**, (2004); S. Mereghetti et al., *Astrophys. J.* **624**, L105 (2005)
- [3] Palmer D.M. et al., *GCN Circ.* **2925**, (2004)
- [4] Hurley K. et al., *Nature* **434**, 1098, (2005)
- [5] Kouveliotou C., Duncan R.C., Thompson C., *Sci. Am.* **288N2** (2003)
- [6] D. M. Palmer et al., *Nature* **434**, 1107 (2005).
- [7] F. Halzen, H. Landsman and T. Montaruli, eprint: astro-ph/0503348 and updated paper in preparation.
- [8] J.D. Gelfand et al., *Astrophys. J.* **634**, 89 (2005).
- [9] K. Ioka et al., *Astrophys. J.* **633**, 1013 (2005).
- [10] E. Andrés et al., *Astrop. Phys.* **13**, 1 (2000).
- [11] T. Terasawa et al., eprint: astro-ph/0502315, subm. to *Nature*.
- [12] D. Gotz, private communication.
- [13] E. Pian and S. Schwartz, private communication.
- [14] G. C. Hill, J. Hodges, B. Hughey, A. Karle and M. Stamatikos, Proc. of PHYSTAT 2005, Oxford. G. C. Hill and K. Rawlins, *Astrop. Phys.*, **19**, 393, (2003).
- [15] D. Heck et al., FZKA-6019 (1998).
- [16] A. Gazizov and M.P. Kowalski, *Comput. Phys. Commun.* **172** 203 (2005).

IceCube - First Results

Jon Dumm and Hagar Landsman for the IceCube Collaboration

Department of Physics, University of Wisconsin, Madison, Wisconsin, USA

E-mail: hagar@icecube.wisc.edu, jdumm@icecube.wisc.edu

Abstract. During the last two austral summers, the first sensors of the IceCube neutrino observatory were deployed in the deep Antarctic ice, along with a surface array. We will present first results obtained using the IceCube detector, demonstrating that the performance is within the design requirements, and showing the ability to reconstruct tracks, cascades and synchronizing times in the entire array to within 3 ns.

1. Introduction

The IceCube detector currently under construction at the South Pole, will consist of up to 4800 Digital Optical Modules (DOMs) covering a fiducial volume of 1 cubic km [1]. The DOMs will be equally spaced on up to 80 strings, at depth from 1.5 to 2.5 km in the deep, clear Antarctic ice. An array of surface stations, IceTop, enhance the ability to trigger on, or veto, down-going showers. Each IceTop station consisted of two clear ice tanks, each instrumented with 2 DOMs. An IceTop station is located roughly 10 meters from each bore hole of the In-Ice array.

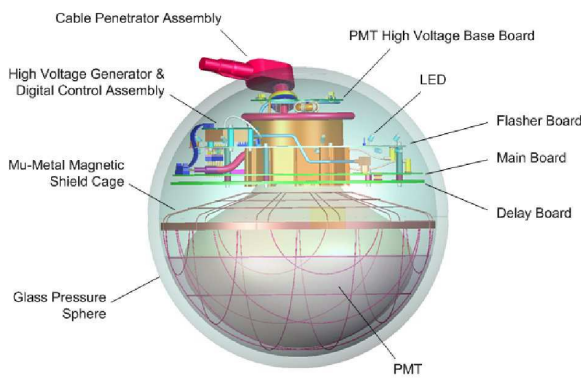


Figure 15. A schematic view of an IceCube Digital Optical Module (DOM)

IceCube is designed to detect Cherenkov radiation photons emitted by charged particles. The particles that are most likely to penetrate through the 1.5 km of ice on top of the detector are muons (from interaction of cosmic rays in the atmosphere), and neutrinos (atmospheric or from any other source). The rate of the muon background is about 6 orders of magnitude larger than that of atmospheric neutrinos, and therefore neutrino searches are performed using up-going particles that traverse the entire earth, using the matter of our planet as a muon screen. Based on measurements of the number of photons arriving at different DOMs and their arrival times, a track or a cascade can be reconstructed. Each

DOM is an autonomous data collecting and analyzing unit consisting of a 10" Hamamatsu PMT in a 12" pressure sphere (see figure 15). A main board inside the DOM can digitize up to 300 Mega Samples per Second (MSPS) for 400 ns and 40 MSPS for $6.4\mu s$. A flasher board, populated with 12 Light Emitting Diodes (LEDs), produces pulses used for optical and timing calibration. The DOMs can operate in a local coincidence mode, where a data recording will be triggered only if its neighbors were triggered within a certain time window.

The main scientific goal of IceCube is to map the neutrino sky [1]. IceCube will also look for high energy GZK neutrinos [2], study air showers, high energy atmospheric neutrinos [3] and look for supernovas in a special data acquisition mode [7]. IceCube measurements can be used, to some extent, also for neutrino mass hierarchy and CP phase measurements [4]. There are models predicting certain neutrino flux enhancements, which could be measured by IceCube. These sources include, but are not limited to, dark matter, super-symmetry, magnetic monopoles, quantum gravity [5].

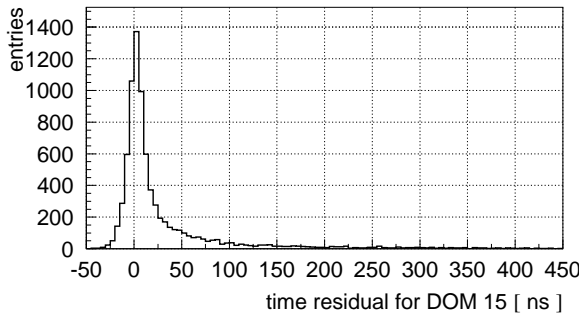


Figure 16. Distribution of time residuals of photons arriving at a DOM from nearby tracks reconstructed with the rest of the string. Photons arriving from the track directly with no scattering will have time residual = 0

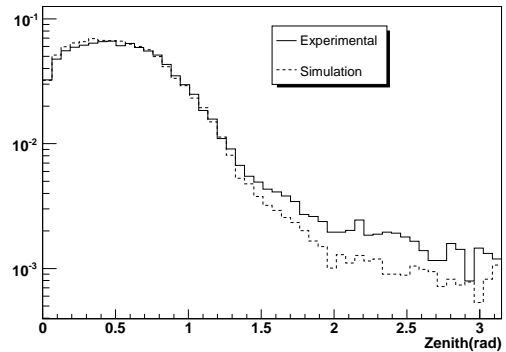


Figure 17. Distribution of reconstructed zenith angle for muon events

2. Current Status and Verification

In the winter of 2004-2005 a single In-Ice string and 4 IceTop stations were deployed. At the end of the 2006 Austral summer IceCube consists of 9 In-Ice strings and 16 IceTop stations. A set of measurements were performed to confirm the design goal of the detector and check its performance [6]. In order to reconstruct and time tracks over the entire array, a timing resolution of a few nanoseconds is needed. The time resolution of each detector unit was estimated in two independent ways. In the first the flasher board was used. A LED on a DOM was flashed and adjacent DOMs triggered on it. The time delay between the flashing and the triggering was measured multiple times. This procedure was repeated for all DOMs, and the maximum time RMS resolution was found to be less than 2ns. A different way to estimate the time resolution is by reconstructing down-going muon tracks excluding one DOM, and calculating the time difference between the measured hit time and the expected hit time. Figure 16 shows the distribution of those time residuals for a single DOM using multiple events. The process is repeated for all DOMs. The resolution was found to be less than 3 ns, after correcting for ice properties.

The distributions of different reconstruction parameters were compared to predicted rates and simulated Monte Carlo events. For both down-going atmospheric muon candidate events, and up-going neutrino candidates events the agreement between Monte Carlo and data was good, and in agreement with previous predictions [8]. A comparison of the zenith angle distributions is shown in figure 17. In order to estimate signal and background behavior and check detector performance, a reliable neutrino interaction and detector simulation is needed. The IceCube simulation software is currently under active development.

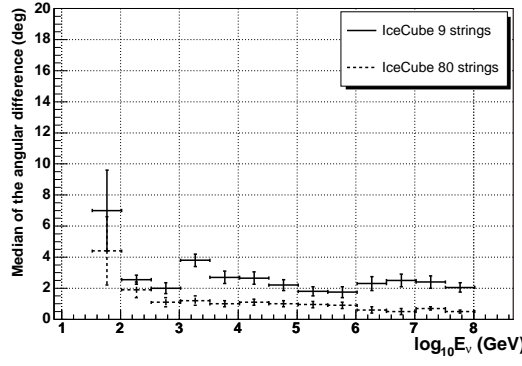


Figure 18. The angular resolution for 9 In-Ice strings and for the full IceCube array as function of event energy (Preliminary). Shown here the differences between the true and reconstructed muon track.

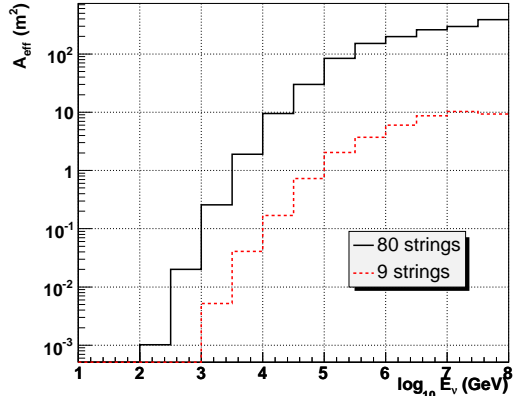


Figure 19. The effective area calculated for 9 and 80 strings detector, for reconstructed muon tracks as function of the neutrino energy (Preliminary)

3. Future Sensitivity

Using simulation of the 9 and 80 string detector configurations, effective areas, angular resolutions and event rates were estimated. Likelihood reconstructions run on simulation are used to estimate the angular resolution of the detector, shown as a function of energy in figure 18. Resolutions can also be characterized by energy spectral indices. For example, the angular resolution for reconstructed atmospheric muon tracks will be about 2.2° (2.7°) using 80 (9) strings, and 0.8° (1.3°) for an E^{-2} spectrum. The angular resolution results quoted are expected to improve when the DOM waveform information will be fully used. In figure 19 the estimated effective area for neutrino detection as function of energy is shown.

References

- [1] IceCube Project Preliminary Design Document, Ahrens et al. (IceCube Collaboration), <http://icecube.wisc.edu>.
- [2] R.Engel, D.Seckel and T.Stanev, Phys.Rev. D64 093010 (2001)
- [3] M.C. Gonzalez-Garcia, F.Halzen and M.Maltoni, Phys.Rev. D71, 092010 (2005).
- [4] W. Winter, Phys.Rev. D74, 033015 (2006)
- [5] L. Anchordoqui et al., Phys. Rev. D72, 065019 (2005) I.F. Albuquerque, G. Burdman and Z. Chako, Phys. Rev. Lett. 92, 221802 (2004) I.F. Albuquerque, J. Lamoreaux and G. Smoot, Phys. Rev. D66, 1215006 (2002)
- [6] A. Achterberg et al. (IceCube collaboration), Astropar. Phys. 26, 155 (2006)
- [7] J.Ahrens et al. (AMANDA Collaboration), Astropart. Phys. 16 , 345 (2002)
- [8] J. Ahrens et al. (IceCube Collaboration), Astropart. Phys. 20 , 507 (2004)

Multi-year search for a diffuse flux of muon neutrinos with AMANDA-II

J. Hodges for the IceCube Collaboration

Department of Physics, University of Wisconsin, Madison, Wisconsin, USA

E-mail: hodges@icecube.wisc.edu

Abstract. A search for TeV to PeV muon neutrinos from unresolved sources was performed on AMANDA-II data collected between 2000 to 2003. The diffuse analysis sought to identify an extraterrestrial neutrino signal on top of the atmospheric muon and neutrino backgrounds. An upper limit of $E^2 \Phi_{90\% C.L.} < 8.8 \times 10^{-8} \text{ GeV cm}^{-2} \text{ s}^{-1} \text{ sr}^{-1}$ was placed on the diffuse flux of muon neutrinos with a $dN/dE \sim E^{-2}$ spectrum for the energy range 15.8 TeV to 2.5 PeV. Limits were also placed on prompt and astrophysical neutrino models with other energy spectra.

1. Introduction

Current theories on cosmic particle acceleration predict that neutrinos and gamma rays are among the by-products of pp and $p\gamma$ interactions in sources such as AGN (active galactic nuclei) or GRBs (gamma ray bursts). Many extraterrestrial TeV gamma ray sources have already been identified by other experiments, but the missing link is the detection of an extraterrestrial neutrino flux. This search was optimized to look for extraterrestrial neutrinos with a $dN/dE \sim E^{-2}$ spectrum, the most general prediction from first order Fermi acceleration models.

A diffuse search for neutrinos does not use specific time or location information. Instead, it looks for an excess of events over a large sky region over a long period of time. If the neutrino flux from an individual source is too small to be detected by current means, it is possible that many similar sources, isotropically distributed throughout the Universe, would combine to make a detectable signal. An excess of events over the expected atmospheric neutrino background would be indicative of an extraterrestrial neutrino flux.

2. Search Methods

Data for this analysis were collected by AMANDA-II between 2000 to 2003. This period covered 807 days of stable detector livetime. During this period, 5.2×10^9 events triggered AMANDA-II.

2.1. Backgrounds for the diffuse analysis

Several types of events that can trigger the detector were simulated. Atmospheric muons and neutrinos created when cosmic rays interact with the Earth's atmosphere are the main background to extraterrestrial neutrino-induced events. Atmospheric and extraterrestrial neutrinos can travel from the far side of the Earth, interact in the ice or rock near the detector, and induce an upward-moving muon that can be detected. Atmospheric muons, on the other hand, do not have enough energy to travel a long distance through the earth, and hence they can only trigger the detector if they travel downward from the polar surface into the ice.

The first step in the analysis was to guess an arrival direction for every event [1], as shown on the left in Figure 20. Using this directional information, all events that were reconstructed in the downgoing

direction were removed. The Earth was used as a filter and the actual search for extraterrestrial neutrinos was only performed on upgoing events.

Since the arrival direction of many downgoing atmospheric muons was originally misreconstructed, event quality requirements were introduced. Events were required to have long, smooth tracks of light that had many Cherenkov photons arriving close to their expected arrival times. This helped remove any misreconstructed downgoing events and helped to assure a purely upgoing sample that can be seen on the right in Figure 20.

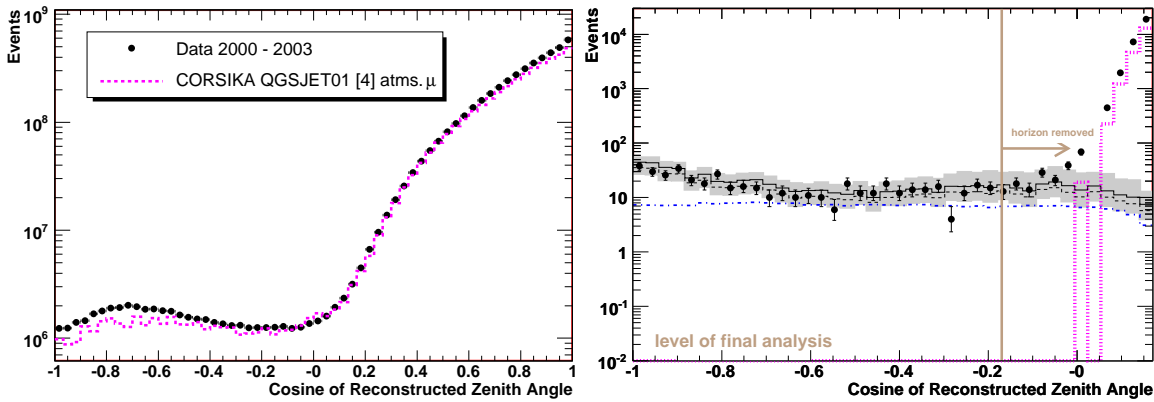


Figure 20. The cosine of the zenith angle is plotted for all events that triggered the detector (left). Events at $\cos(\text{zenith}) = -1$ are traveling straight up through the detector from the Northern Hemisphere. On the right, event quality requirements were used to select the best upgoing tracks. The normalization of the atmospheric neutrino simulation was adjusted so that the number of events hitting between 50 and 100 OMs was the same in the data and simulation.

● Data 2000 - 2003
■ Uncertainty in atmospheric ν flux
— Barr et al. [2] atms. ν
..... Honda et al. [3] atms. ν
··· CORSIKA QGSJET01 [4] atms. μ
··· Signal ν : $E^2\phi = 10^6 \text{ GeV cm}^2 \text{ s}^{-1} \text{ sr}^{-1}$

2.2. Separating atmospheric neutrinos from extraterrestrial neutrinos

Atmospheric neutrinos from pions and kaons ($dN/dE \sim E^{-3.7}$) have a softer energy spectrum than the proposed extraterrestrial neutrino signal ($dN/dE \sim E^{-2}$). As a result, these two event classes can be separated best by their energy. At high energy, the extraterrestrial neutrino flux would dominate over the atmospheric neutrinos.

Since the energy of an event is not directly observable, the number of optical modules (OMs) hit during an event was used as an energy-correlated parameter. Optimization studies performed on the simulation indicated that the best signal-to-background region would be obtained by using events with at least 100 OMs triggered. The number of data events seen in this high energy window was compared to the predicted atmospheric neutrino background, shown in Figure 21.

3. Systematic uncertainties

An extensive systematic uncertainty analysis was performed to include uncertainties in the neutrino flux models and detector performance. Two different atmospheric neutrino models were used, Barr *et al.* [2] and Honda *et al* [3]. Uncertainties in the cosmic ray flux and the hadronic interaction model were also considered. All of the atmospheric neutrino simulation was scaled so that the number of simulation events matched the number of data events in the region $50 < \text{number of OMs hit} < 100$.

To assess detector and simulation performance, an inverted analysis was performed in which the highest quality downgoing events were studied. Downgoing events that were previously eliminated ($0^\circ < \text{zenith angle} < 80^\circ$) were reintroduced. With very high statistics available from these downgoing events,

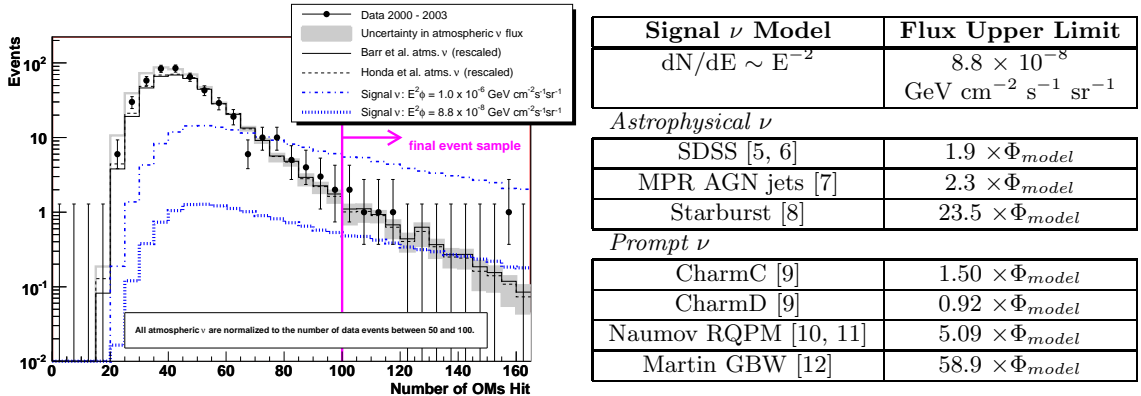


Figure 21. (Left) The number of OMs triggered during each event is an energy-correlated observable. Events triggering at least 100 OMs appeared in the final data set, and the number of observed data events was compared to the simulated atmospheric neutrino background. (Right) Upper limits were also determined for flux models (Φ_{model}) with different energy spectra.

the characteristics of high energy events were studied without having to reveal the high energy upgoing data events.

4. Results

Six data events were observed on an average predicted atmospheric neutrino background of 6.1 events. Since no excess of events was seen indicating an extraterrestrial signal, an upper limit was set for a $dN/dE \sim E^{-2}$ flux between 15.8 TeV to 2.5 PeV (the energy region covered by 90% of the simulated signal). The upper limit on the diffuse flux of muon neutrinos from AMANDA-II data from 2000 to 2003 is $E^2\Phi_{90\%C.L.} < 8.8 \times 10^{-8} \text{ GeV cm}^{-2} \text{s}^{-1} \text{sr}^{-1}$.

Signal models with other energy spectra were also tested with this data. Due to the different nature of their energy spectra, the requirement of how many OMs were triggered during an event was reoptimized. The upper limit on each of the models appears in the table above.

References

- [1] Ahrens J *et al* 2004 *Nucl. Instr. Meth. A* **524** 169
- [2] Barr GD, Gaisser TK, Lipari P, Robbins S and Stanev T 2004 *Phys. Rev. D* **70** 023006
- [3] Honda M, Kajita T, Kasahara K and Midorikawa S 2004 *Phys. Rev. D* **70** 043008
- [4] Heck D, Knapp J, Capdevielle JN, Schatz G and Thouw T 1998 Tech. Rep. FZKA 6019 Forschungszentrum Karlsruhe
- [5] Stecker FW, Salamon MH, Done C and Sommers P 1992 *Phys. Rev. Lett.* **66** 2697 (1991), **69** 2738(E)
- [6] Stecker FW 2005 *Phys. Rev. D* **72** 107301
- [7] Mannheim K, Protheroe RJ and Rachen JP 2000 *Phys. Rev. D* **63** 023003
- [8] Loeb A and Waxman E 2006 *J. Cosmol. Astropart. Phys.* JCAP05 003
- [9] Zas E, Halzen F and Vázquez RA 1993 *Astropart. Phys.* **1** 297
- [10] Fiorentini G, Naumov A and Villante FL 2001 *Phys. Lett. B* **510** 173
- [11] Bugaev EV *et al* 1989 *Il Nuovo Cimento* 12C, No. 1, 41
- [12] Martin AD, Ryskin MG and Stasto AM 2003 *Acta Phys. Polon. B* **34** 3273

Searches for Neutrinos from Gamma Ray Bursts with AMANDA-II and IceCube

B. Hughey for the IceCube Collaboration

Department of Physics, University of Wisconsin, Madison, Wisconsin, USA

E-mail: hughey@icecube.wisc.edu

Abstract. The hadronic fireball model predicts a neutrino flux in the TeV to several PeV range simultaneous with the prompt photon emission of GRBs. The discovery of high energy neutrinos in coincidence with a gamma ray burst would help confirm the role of GRBs as accelerators of high energy cosmic rays. We summarize the methods employed by the AMANDA experiment in the search for neutrinos from GRBs and present results from several analyses.

1. Neutrinos From GRBs

Gamma Ray Bursts (GRBs) are one of the most plausible sources of ultra-high energy cosmic rays [1, 2]. Detection of high energy neutrinos from a burst would provide corroborating evidence for the production of ultra-high energy cosmic rays inside GRBs.

It is believed that gamma rays produced by GRBs originate from electrons accelerated in internal shock waves associated with relativistic jets (with Lorenz boost $\Gamma \sim 300$). These gamma rays have energies in the range from 10 keV to greater than 10 MeV. The gamma ray spectrum can be described as a broken power law, with a softer spectrum above a break energy which is typically 0.25-1 MeV. Gamma ray bursts can last anywhere from a few milliseconds up to a few hundred seconds. The distribution of durations is usually considered to be composed of two separate classes, with short bursts lasting less than 2 seconds and long bursts lasting more than 2 seconds [3]. Gamma ray bursts are reviewed in [4] and [5].

If protons and/or nuclei are also accelerated in the jets, then high energy neutrinos ($\sim 10^{14}$ eV) are produced [1] via the process:

$$p + \gamma \rightarrow \Delta^+ \rightarrow \pi^+[+n] \rightarrow \nu_\mu + \mu^+ \rightarrow \nu_\mu + e^+ + \bar{\nu}_\mu + \nu_e. \quad (7)$$

The neutrino flavor ratio $\nu_e:\nu_\mu:\nu_\tau$ is thus 1:2:0 at source. Taking into account neutrino oscillations, the flavor ratio observed at Earth is 1:1:1 [6]. However, Kashti and Waxman [7] point out that at energies greater than ~ 1 PeV, the μ^+ in Equation (7) loses energy through synchrotron radiation before decaying. This energy loss changes the source neutrino flavor ratio at high energies from 1:2:0 to 0:1:0, leading to a ratio at Earth of 1:1.8:1.8.

Neutrino production is predicted to be simultaneous with gamma ray production. AMANDA GRB analyses use the Waxman-Bahcall [1] broken power law neutrino spectrum as a reference hypothesis (see Fig. 1). However, other models of prompt neutrino emission have also been tested. These include the parameterization of Murase and Nagataki [8], who arrive at a similar spectrum to Waxman-Bahcall under different assumptions, as well as the supernova scenario (now disfavored due to evidence from the Swift satellite) which assumes GRB jet interactions with an external matter field created by a supernova preceding the burst by ~ 1 week [9]. Predictions have also been made for precursor [10] and afterglow [11] emission.

2. The AMANDA Detector

The Antarctic Muon and Neutrino Detector Array (AMANDA) [12, 13] is located at the South Pole. From 1997 to 1999, AMANDA consisted of 302 optical modules on 10 strings and was referred to as AMANDA-B10. The final configuration, AMANDA-II, was commissioned in the year 2000 and consists of a total of 677 optical modules on 19 strings. Each module contains a photomultiplier tube and supporting hardware inside a pressurized glass sphere. The optical modules are used to indirectly detect neutrinos by measuring the Cherenkov light from secondary charged particles produced in neutrino-nucleon interactions.

AMANDA uses two detection channels. Muon tracks are produced through interactions of ν_μ , while cascades (particle showers) are produced from interactions of all three neutrino flavors. The muon channel has a larger effective areas because of the longer range of muons compared to cascades. It also has better pointing resolution because muons produce linear tracks rather than spherical showers. Separating neutrino signals from the dominant atmospheric muon background is accomplished by removing downgoing events, so muon analyses have $\sim 2\pi$ sr sky coverage. Cascades are differentiated from downgoing muons by their shape and therefore cascade analyses have full (4π sr) sky coverage. Cascade events also have better energy resolution than muon tracks, since the energy of all particles produced in the shower is accounted for.

3. AMANDA GRB Analyses

In the majority of GRB analyses, searches are done in coincidence with γ -ray detections by satellites. Because these analyses only search for a neutrino signal during the time and (in the case of muon channel searches) in the location of measured bursts, there is almost no on-source background in these analyses. The period of time actually examined for a neutrino signal for each burst is equal to the measured duration of prompt gamma-ray emission, plus the uncertainty in this measurement, plus an additional second on each side of the on-time window. Background was measured for a period of one hour both before and after each burst, with the ten minute period immediately surrounding the burst remaining unexamined to avoid the possibility of contaminating the background with neutrino signal. In the muon channel, searches for prompt emission have been conducted for 312 bursts measured by the BATSE detector (aboard the CGRO satellite) and 95 bursts analyzed by the IPN3 satellite. Additionally, a search for precursor emission was conducted using 60 bursts from the 2001-2003 data sets [14]. Using the cascade channel, 73 bursts identified by the BATSE detector in the year 2000 have been studied [15]. No events have been observed in coincidence with any bursts studied so far, which is consistent with the expected background.

The *rolling* analysis provides a useful complement to these triggered searches. This method does not use satellite triggers, but scans an entire multi-year data sample for a statistical excess of events within one of two pre-set time windows (to account for both long and short burst classes). This allows this analysis to search for GRBs and other transients not identified by satellites. The rolling search has been conducted for the years 2001-2003 (after the BATSE detector was ceased operations and before the Swift satellite launched) using the cascade channel. Due to the larger amount of data analyzed relative to the triggered analyses, more stringent cuts on the data are required. Thus, background rejection was accomplished with a six cut-variable Support Vector Machine, optimized for the best chance for signal discovery. As in the case of the triggered searches, no evidence of astrophysical neutrinos has been found with this analysis method. The maximum number of observed events and the numbers of observed windows with multiple (2 or 3) events is consistent with the predicted background [15].

Although the Waxman-Bahcall neutrino spectrum functions as a reference for GRB analyses, it has been demonstrated that neutrino spectra from individual bursts can vary significantly from this “standard” spectrum [16, 17]. Current AMANDA analyses are using more sophisticated methods to predict the spectrum and neutrino rates for individual bursts rather than assuming averaged parameters. The particularly close and bright burst GRB030329 was the first burst to be given this individualized treatment [18]. Bursts detected by Swift, many of which have redshifts directly measured from afterglow data, will be especially conducive to this method.

IceCube, the successor to AMANDA, is currently under construction, with the final detector scheduled be completed by 2011. Preliminary studies indicate that a triggered search using 300-500 bursts with the full IceCube array would suffice to either set limits at levels lower than the predictions by Waxman-Bahcall or find evidence of the existence of neutrinos in coincidence with GRBs with better than 5σ

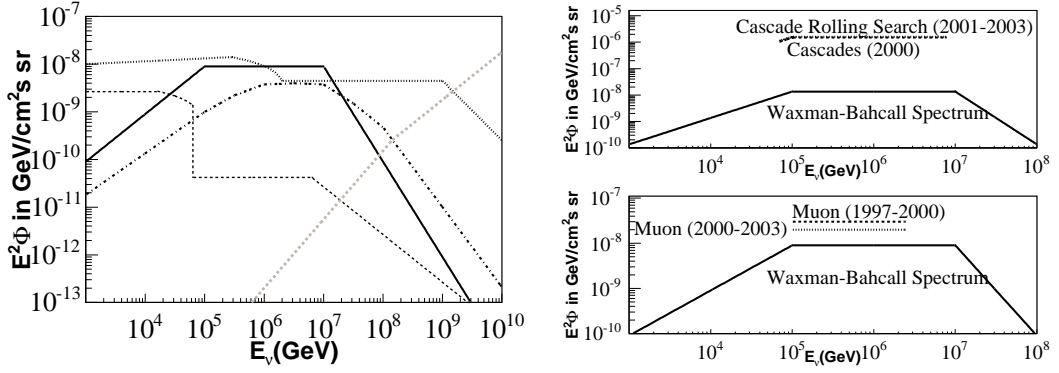


Figure 22. Left: Models of neutrino emission from GRBs: Solid: Waxman-Bahcall; Dotted: Supernova; Dash-Dotted: Murase-Nagataki; Light Dashed: Afterglow; Dark Dashed: Precursor Emission. Right: Experimental limits relative to Waxman Bahcall spectrum for cascade (top) and muon (bottom) channels, with displayed ranges containing 90% of simulated signal events.

confidence.

References

- [1] Waxman E and Bahcall J 1997, *Phys. Rev. Lett.* 78, 2292
- [2] Wick S, Dermer C D and Atoyan A 2004, *Astropart. Phys.* 21, 125
- [3] Paciesas W S et al. 1999, *ApJS* 122, 465 (astro-ph/9903205)
<http://www.batse.msfc.nasa.gov/batse/grb/catalog/>
- [4] Meszáros P 2006, *Rept. Prog. Phys.* 69, 2259
- [5] Piran T 2005, *Rev. Mod. Phys.* 76, 1143
- [6] Athar H, Kim C S and Lee J 2006, *Mod. Phys. Lett. A* 21, 1049
- [7] Kashti T and Waxman E 2005, *Phys. Rev. Lett.* 95, 181101
- [8] Murase L and Nagataki S 2006, *Phys. Rev. D* 73, 063002
- [9] Razzaque S, Meszáros P and Waxman E 2003, *Phys. Rev. Lett.* 90, 1103
- [10] Meszáros P and Waxman E 2001, *Phys. Rev. Lett.* 87, 17110
- [11] Waxman E and Bahcall J 2000, *ApJ* 541, 707
- [12] Andrés E et al. 2001, *Nature* 410, 441
- [13] Woschnagg K et al. 2005, *Nuclear Physics B Proc. Suppl.* 143, 343
- [14] Kuehn K et al. 2005, in Proc 29th Int. Cosmic Ray Conf. (in astro-ph/0509330)
- [15] Hughey B et al. 2005, in Proc 29th Int. Cosmic Ray Conf. (in astro-ph/0509330)
- [16] Becker J et al. 2006, *Astropart. Phys.* 25, 118-128
- [17] Guetta D et al. 2004, *Astropart. Phys.* 20, 429
- [18] Stamatikos M et al. 2005, in Proc 29th Int. Cosmic Ray Conf. (in astro-ph/0509330)

Acknowledgments We acknowledge the support from the following agencies: National Science Foundation-Office of Polar Program, National Science Foundation-Physics Division, University of Wisconsin Alumni Research Foundation, Department of Energy, and National Energy Research Scientific Computing Center (supported by the Office of Energy Research of the Department of Energy), the NSF-supported TeraGrid system at the San Diego Supercomputer Center (SDSC), and the National Center for Supercomputing Applications (NCSA); Swedish Research Council, Swedish Polar Research Secretariat, and Knut and Alice Wallenberg Foundation, Sweden; German Ministry for Education and Research, Deutsche Forschungsgemeinschaft (DFG), Germany; Fund for Scientific Research (FNRS-FWO), Flanders Institute to encourage scientific and technological research in industry (IWT), Belgian Federal Office for Scientific, Technical and Cultural affairs (OSTC); the Netherlands Organisation for Scientific Research (NWO); M. Ribordy acknowledges the support of the SNF (Switzerland); J. D. Zornoza acknowledges the Marie Curie OIF Program (contract 007921).

